

## The Intrinsic Flattening of Extragalactic Stellar Disks

JEREMY FAVARO,<sup>1</sup> STÉPHANE COURTEAU,<sup>1</sup> SÉBASTIEN COMERÓN,<sup>2,3</sup> AND CONNOR STONE<sup>4,5,6</sup>

<sup>1</sup>*Department of Physics, Engineering Physics & Astronomy, Queen's University, Kingston, ON K7L 3N6, Canada*

<sup>2</sup>*Departamento de Astrofísica, Universidad de La Laguna, 38200 La Laguna, Tenerife, Spain*

<sup>3</sup>*Instituto de Astrofísica de Canarias, 38205 La Laguna, Tenerife, Spain*

<sup>4</sup>*Department of Physics, Université de Montréal, Montréal, Québec, Canada*

<sup>5</sup>*Mila - Québec Artificial Intelligence Institute, Montréal, Québec, Canada*

<sup>6</sup>*Ciela - Montréal Institute for Astrophysical Data Analysis and Machine Learning, Montréal, Québec, Canada*

### ABSTRACT

Highly inclined (edge-on) disk galaxies offer the unique perspective to constrain their intrinsic flattening,  $c/a$ , where  $c$  and  $a$  are respectively the vertical and long radial axes of the disk measured at suitable stellar densities. The ratio  $c/a$  is a necessary quantity in the assessment of galaxy inclinations, three-dimensional structural reconstructions, total masses, as well as a constraint to galaxy formation models.  $3.6\ \mu\text{m}$  maps of 133 edge-on spiral galaxies from the Spitzer Survey of Stellar Structure in Galaxies (S<sup>4</sup>G) and its early-type galaxy extension are used to revisit the assessment of  $c/a$  free from dust extinction and away from the influence of a stellar bulge. We present a simple definition of  $c/a$  and explore trends with other galactic physical parameters: total stellar mass, concentration index, total H I mass, mass of the central mass concentration, circular velocity, model-dependent scales, as well as Hubble type. Other than a dependence on early/late Hubble types, and a related trend with light concentration, no other parameters were found to correlate with the intrinsic flattening of spiral galaxies. The latter is mostly constant with  $\langle c/a \rangle = 0.124 \pm 0.001$  (stat)  $\pm 0.033$  (intrinsic/systematic) and greater for earlier types.

*Keywords:* Galaxy disks, Galaxy dynamics, Galaxy kinematics, Galaxy properties, Galaxy structure

### 1. INTRODUCTION

Stellar disks viewed edge-on display a distinct thickness characterized by an intrinsic flattening,  $c/a$ . Knowledge and modeling of the latter is important for understanding galaxy structure (Comerón et al. 2012; Díaz-García et al. 2022), accretion history (Toth & Ostriker 1992; Buck et al. 2020; Hopkins et al. 2023), galaxy evolution (Kautsch et al. 2009; Meng & Gnedin 2021; García de la Cruz et al. 2023), constraining numerical simulations (Meng & Gnedin 2021; Sotillo-Ramos et al. 2022; Hopkins et al. 2023), and more. Beyond the physical understanding of galaxy flattening, the determination of  $c/a$  directly affects galaxy inclinations, which are themselves critical for the deprojection of observables such as line widths, rotation curves, and light profiles, among others, from which global galaxy structural parameters may be estimated. For instance, estimates of galaxy mass and surface brightness profile decompositions, e.g., into the sum of a bulge and disk components, rely on suitable value(s) of  $c/a$ .

Historically, the determination of  $c/a$  has employed a statistical analysis of the apparent  $c/a$  distribution for large galaxy samples with all projected inclinations yielding an extrapolated intrinsic  $c/a$  distribution (e.g., Holmberg 1946; Sandage et al. 1970; Guthrie 1992; Lambas et al. 1992; Giovanelli et al. 1994; Unterborn & Ryden 2008). This approach was typically justified by assuming that (i) disk galaxies are oblate spheroids and (ii) that the intrinsic  $c/a$  distribution should be Gaussian. The former assumption is too restrictive (disk galaxies are slightly triaxial; Lambas et al. 1992; Fasano et al. 1993; Alam & Ryden 2002; Ryden 2004) while the latter is fair.

Measurements of  $c/a$  have also been ill-characterized, especially for older values based on photographic plates whose limiting isophotes were constrained by the sensitivity of the plates (de Vaucouleurs et al. 1964; Nilson 1973). Measurements of  $a$  and  $c$  have often been made at arbitrary locations (see Trujillo et al. 2020, for an in-depth discussion). To remedy this issue, we define the location of  $c$  relative to  $a$  by way of “characteristic cuts”, which consist of rigorous and reproducible measurements of  $c/a$  for any disk galaxy observed with a digital detector (detailed in Sec. 4.1). Our study attempts to provide such a rigorous, straightforward, definition of  $c/a$ , free of extinction effects and the influence of a bulge, for accurate astrophysical applications as well as comparisons with numerical models of disk galaxies.

Model-dependent axis ratios, like the ratio of disk scale height,  $z$ , to scale length,  $h$ , have occasionally been used in lieu of  $c/a$  as a measure of true disk thickness (e.g., Kregel et al. 2004; Padilla & Strauss 2008; Stark et al. 2009; van der Wel et al. 2012; Mosenkov et al. 2015; Shibuya et al. 2015; Doore et al. 2021). This approach alleviates the need for a specific measurement location for  $c$ . However, significant drawbacks of this approach are that the adopted model to estimate scale parameters, whether in length or height, may not be realistic and may be arbitrarily complex (e.g., given bars, breaks, lenses, and model parameterizations). For instance, exponential disk models representing the radial light drop-off of luminous disks with parametric scale lengths,  $h$ , have often been invoked for disk galaxies (e.g., Freeman 1970; Kregel et al. 2002; Erwin et al. 2005; Hernandez & Cervantes-Sodi 2006; Erwin et al. 2008). However, offsets from this model can be significant (Erwin et al. 2005; Pohlen & Trujillo 2006; Erwin et al. 2008; Comerón et al. 2018; Mosenkov et al. 2022). Similar concerns hold for vertical profiles, whether exponential with scale height  $z_0$ ,  $\text{sech}^2$  with scale height  $z_{\text{sech}^2} = 2z_0$  (e.g., van der Kruit & Searle 1981; de Grijs 1998; Yoachim & Dalcanton 2006; Mosenkov et al. 2015), or Sérsic models (van der Wel et al. 2012). Given the many assumptions in any model-dependent fit, such practice requires great care in execution and application.

One-dimensional (1D) parametric decompositions targeted at retrieving intrinsic disk flattening require careful consideration of bulge light. For example, de Grijs (1998)’s 1D reduction reported  $\langle z_0/h \rangle \sim 0.15$  for spiral galaxies, yet 1D photometric profiles were found to overestimate  $z_0/h$  (Kregel et al. 2002), especially in galaxies with large bulges (Mosenkov et al. 2015). Both Kregel et al. (2002) and Mosenkov et al. (2015) performed two-dimensional (2D) bulge-disk decompositions on spirals and reported  $\langle z_0/h \rangle \sim 0.13$ . The three-dimensional (3D) SB profile decompositions of Mosenkov et al. (2022) found even thinner stellar disks with  $\langle z_0/h \rangle \sim 0.1$  at  $3.4 \mu\text{m}$ . In what follows, comparisons between our model-independent approach and model-dependent results will be presented.

Our paper is organised as follows. Our brief historical review in Sec. 2 reveals that most previous measurements of  $c/a$  have largely relied on ground-based blue sensitive, and thus dust-extinction prone, material and lacked a precise definition of the  $c$  and  $a$ . We suggest a method based on infrared digital surveys of disk galaxies. In Sec. 3, we present the data used in our analysis, ranging from science-ready images to disk decompositions from other works. Our data reduction methodology to identify isophotes that characterise the disk’s structure, as well as relevant statistical concerns, are addressed in Sec. 4. Results are presented in Sec. 5. The shape of the intrinsic flattening distribution, and whether it is normal, is considered along with correlations between our (model-independent)  $c/a$  values and structural galaxy properties, including similar measures from parametric (model-dependent) disk decompositions. We also test for any biases due to galactic environments. A discussion of our main findings is presented in Sec. 6, including a discussion contrasting model-independent and model-dependent estimates of intrinsic flattening. Future avenues are discussed in Sec. 7 and followed by a summary in Sec. 8. App. A discusses potential resolution effects on the measurement of  $c/a$ .

## 2. HISTORICAL REMARKS

Measurements of  $c/a$  yield galaxy inclinations via Hubble’s formula for oblate spheroids (Hubble 1926):

$$\cos^2 i = \frac{q^2 - (c/a)^2}{1 - (c/a)^2}, \quad (1)$$

where  $i$  is the inclination,  $q$  is the observed flattening, and  $a$  and  $c$  are the semi-major and semi-minor axes of the disk, respectively. In all but edge-on views, the intrinsic flattening is never observed. The intrinsic thickness,  $c/a$ , of a galaxy disk is also ideally measured at a given surface density (brightness) level or fiducial location.

Early estimates of  $c/a$  relied on measuring apparent galaxy sizes off of photographic plates. The latter were mostly sensitive to blue light and thus affected by dust extinction. Holmberg (1946) developed a model to map the distribution of observed versus intrinsic axial ratios for idealized spiral galaxies whose true axis ratios and inclinations were known. This model was then applied to a collection of 156 disk galaxies to infer an estimate for their intrinsic  $c/a = 0.2$  after assuming that  $\cos i$  follows a uniform distribution. The axial ratios  $a$  and  $c$  were measured visually at the observed galaxy edges by Holmberg and colleagues.

Sandage et al. (1970) also studied the morphological dependence of  $c/a$  for 168 elliptical, 267 lenticular, and 254 spiral galaxies imaged on  $B$ -band photographic plates. These authors fitted various distribution functions to the observed distributions of randomly inclined sample galaxies in order to determine the intrinsic  $c/a$ . The semi-minor and semi-major axes for each galaxy were taken from the RC1 catalogue (de Vaucouleurs et al. 1964). The Gaussian distribution of  $c/a$  for both the spiral and lenticular galaxies had a mean  $\langle c/a \rangle = 0.25$  and a deviation of 0.06.

Other tabulations of  $c/a$  for local disk galaxies include a private correspondence from B.M. Lewis in Haynes & Giovanelli (1984, hereafter HG84). Their Section IV (e) reports a distribution of  $c/a$  ranging from 0.10 for late spirals to 0.23 for lenticulars. Details about the measurements of  $c/a$  were not disclosed. Note that the tabulated values in HG84 are reported and compared with our modern estimates in Table 3 below.

Guthrie (1992) studied 888 isolated disk (Sa to Sc) galaxies from the Uppsala Catalogue of Galaxies (Nilson 1973) to infer a distribution of intrinsic  $\langle c/a \rangle = 0.11 \pm 0.03$ . As with earlier plate-based measurements,  $a$  and  $c$  were measured visually to the edge of each observed galaxy. Guthrie asserted that these visual measurements correlated well with isophotal diameters at the 25  $B$ -band mag arcsec $^{-2}$  isophote.

Instead of considering a particular isophote, Lambas et al. (1992) defined the observed axial ratio using ellipticity values derived from density-weighted image moments, yielding a density-weighted apparent flattening. These authors applied their method to a sample of 13,482 spiral, 4782 lenticular, and 2135 elliptical galaxies imaged in the  $J$ -band and digitized from plates by Loveday (1989). Under the assumption that axis lengths follow a Gaussian distribution, they constructed a triaxial model for the spirals and lenticulars via Monte Carlo simulations. Ultimately, Lambas et al. (1992) reported  $\langle c/a \rangle \approx 0.2$  for spirals and  $\langle c/a \rangle \approx 0.5$  for lenticulars. Their large values were likely biased by stray light from a spheroidal component like a bulge.

Giovanelli et al. (1994) used digital  $I$ -band images of 1235 Sbc and Sc galaxies to measure  $c/a$  at the 23.5 mag arcsec $^{-2}$  isophote. Their model of the observed flattening distribution, which does not depend on an explicit distribution function, produced a best fit  $c/a$  value of 0.13, however the authors suggest that the true mean  $c/a$  ought to be  $\sim 0.10$ . No uncertainty on  $c/a$  was quoted and their model’s standard deviation is especially small. It is interesting that Guthrie (1992) and Giovanelli et al. (1994) reported similar values ( $\langle c/a \rangle = 0.11 - 0.13$ ), despite the former relying on a magnifying glass, upon which a measuring scale was printed, and the latter using digital measurements to measure axis ratios.

More recent investigations on this topic are scanty, with a study by Unterborn & Ryden (2008) standing out. They constructed a sample of 16,155 late-type spiral galaxies from the sixth data release of the Sloan Digital Sky Survey (York et al. 2000; Adelman-McCarthy et al. 2008). Measuring  $c/a$  at the  $r$ -band 25 mag arcsec $^{-2}$  isophote and following the statistical method of Sandage et al. (1970), Unterborn & Ryden (2008) found  $\langle c/a \rangle \approx 0.22$  for slightly triaxial disks.

Overall, published values of  $c/a$  (intrinsic) for disk galaxies have ranged between 0.1 and 0.25. We are revisiting measurements of  $c/a$  since: (i) no previous study of  $c/a$  relied on dust-free (transparent), sky-free, digital images of disk galaxies; (ii) a precise definition of  $a$  and  $c$  (or choice of a sensible distribution function) was seldom provided; (iii) formal errors on  $c/a$  were rarely assessed.

The definition of an unbiased estimate of the “true” flattening of disk systems is challenging since disks are not monolithic slabs; within the optical radius, the vertical height of a disk decreases (often exponentially) with galactocentric radius (e.g., van der Kruit & Searle 1981; de Grijs et al. 1997; de Grijs 1998; van der Kruit & Freeman 2011; Bizyaev et al. 2014), and may increase again in the outskirts due to disk flaring or warping (Olling 1995; Ossa-Fuentes et al. 2023). Of issue then is the availability and widespread application of a rigorous definition of  $a$  and  $c$  which appropriately describes the disk.

Because parametric decompositions (Kregel et al. 2004; Mosenkov et al. 2015; Erwin 2015) are subjective and generally non-unique (Knapen & van der Kruit 1991; MacArthur et al. 2003; Arora et al. 2021), we favour direct measurements of  $c/a$  for an assessment of intrinsic flattening from edge-on systems since surfaces of constant density, whether by light or stellar mass, can be measured and reported unambiguously.

With the availability of digital infrared surveys of the local galaxies, such as the volume-limited *Spitzer* Survey of Stellar Structures in Galaxies (S $^4$ G; Sheth et al. 2010; Muñoz-Mateos et al. 2015; S4G Team 2020), it becomes possible to study the intrinsic flattening,  $c/a$ , of disk galaxies and address the main issues above in a reliable and repeatable manner. The aim of the current study is to provide a straightforward non-parametric measurement of intrinsic flattening for any disk galaxy, based on reliable statistical methods and an extinction-free collection of edge-on galaxies.

Hubble Class	Morphological Classification	Hubble Type	# of Sample Galaxies
Lenticular Galaxies	S0 <sup>-</sup>	-3	7
	S0 <sup>o</sup>	-2	23
	S0 <sup>+</sup>	-1	12
	S0/a	0	8
Spiral Galaxies	Sa	1	1
	Sab	2	5
	Sb	3	4
	Sbc	4	7
	Sc	5	13
	Scd	6	14
	Sd	7	27
	Sdm	8	7
Sm	9	5	

**Table 1.** Morphological classifications of the S<sup>4</sup>G galaxies used in this study, as per the CVRHS system, and number of galaxies of each morphology within our sample.

### 3. DATA

#### 3.1. *The Spitzer Survey of Stellar Structures in Galaxies Sample*

To assess the intrinsic flattening of galactic stellar disks, we have used images from the volume-limited S<sup>4</sup>G and its extended sample of supplementary early-type galaxies ( $T < 0$ ) (Watkins et al. 2022). The latter extended sample enables a valuable representation of lenticular galaxies. The S<sup>4</sup>G is a survey of 2352 galaxies within a radial distance of  $\sim 40$  Mpc ( $z \leq 0.01$ ) observed with the infrared array camera (IRAC; Fazio et al. 2004) onboard the *Spitzer* Space Telescope (Werner et al. 2004) at 3.6 and 4.5  $\mu\text{m}$  wavelengths. The S<sup>4</sup>G is magnitude-limited with  $m_{B\text{CORR}} < 15.5$ , and size-limited to angular scales greater than  $1'$ . The S<sup>4</sup>G's deep imaging reaches an AB surface brightness of  $\mu_{3.6\mu\text{m}} \approx 26$  mag arcsec<sup>-2</sup>. This provides deep infrared views of the stellar disk (unmatched from the ground) and its mass distribution, largely unaffected by dust extinction (Rix & Rieke 1993; Conroy 2013; Courteau et al. 2014). The S<sup>4</sup>G can be broadly viewed as an unbiased survey of local disk galaxies.

For the sake of this study, the S<sup>4</sup>G survey was further restricted to a sub-sample of visually selected systems, yielding a sub-sample of 141 edge-on S<sup>4</sup>G disk galaxies. Details of that selection are found in Comerón et al. (2018). A further 8 galaxies were removed from this sub-sample, as described in Sec. 4.2, resulting in a final sample size of 133 transparent edge-on S<sup>4</sup>G galaxies for this study.

S<sup>4</sup>G galaxies were classified according to the CVRHS system by Buta et al. (2015), with updated  $T$ -type classifications (Watkins et al. 2022). The morphological distribution of galaxies of each  $T$ -type (and corresponding morphology) in our sample is presented in Table 1. It should be noted that galaxy classification of edge-on systems is especially problematic, though the reduced dust extinction in the IRAC bandpass is a significant improvement for this task over bluer dust-prone images. Identifying barred systems in edge-on cases is also challenging, unless a peanut bulge is clearly seen. However, as seen in Sec. 5.1, barredness does not play a role in our assessment of  $c/a$ .

#### 3.2. *Scale Parameters*

As described below (Sec. 4.1), our non-parametric method to estimate the intrinsic flattening,  $c/a$ , of galaxy disks relies on isophotal fitting of (transparent) galaxy images. Galaxy surface brightness (SB) profiles, obtained from radial cuts for edge-on systems, can also be used to measure relevant structural parameters such as the disk scale height,  $z_0$ , and scale length,  $h$ , and to isolate substructure. We will compare in Sec. 5 our non-parametric method of measuring  $c/a$  to the parametric ratio of  $z_0$  and  $h$ , the disk scale height and length. To this end, we have used Comerón et al. (2018)'s decompositions of (major axis) SB profiles for our S<sup>4</sup>G galaxies to source values of the scale heights for the thin and thick disks. We have also extracted disk scale lengths from the (major axis) SB profiles of our S<sup>4</sup>G galaxies by fitting a single exponential to the disk-dominated regions of the profiles.

### 3.3. Global Parameters

In forthcoming sections (Sec. 5.2 and beyond), we will compare our estimates of  $c/a$  with a selection of global physical galaxy parameters in order to explore any correlations. These global parameters include the total stellar mass,  $M_*$ ; the central light concentration index,  $C_{31}$ ; the total H I mass,  $M_{\text{HI}}$ ; the central mass concentration (CMC) mass,  $M_{\text{CMC}}$ ; and the circular velocity,  $V_{\text{rot}}$ . Because our galaxies are viewed edge-on, corrections to  $V_{\text{rot}}$  for inclination were not applied.

The stellar masses,  $M_*$ , were derived for the entire S<sup>4</sup>G sample by Muñoz-Mateos et al. (2015). Their computation assumed a global stellar  $M_*/L$  of  $M/L_{3.6 \mu\text{m}} \approx 0.6 (M_\odot/L_\odot)$  (Meidt et al. 2014). The uncertainty in the adopted  $M/L$  is large as estimates for  $M/L$  ratios in this band range from 0.2 – 0.6  $M_\odot/L_\odot$  (Eskew et al. 2012; Conroy 2013; Courteau et al. 2014; Cluver et al. 2014; Meidt et al. 2014; Hall et al. 2018). Muñoz-Mateos et al. (2015) also provided a concentration parameter  $C_{31}$ , which serves as a proxy for the bulge-to-disk luminosity ratio.  $C_{31}$  is a non-parametric structural parameter defined as the ratio between the radii that enclose 75%,  $r_{75}$ , and 25%,  $r_{25}$ , of the total light of a galaxy.

Our  $M_{\text{HI}}$  values were derived via the basic relation (Giovanelli & Haynes 1988)

$$\begin{aligned} M_{\text{HI}} &= 2.356 \times 10^5 D^2 \left[ \frac{M_\odot}{\text{Mpc}^2 \text{ Jy km s}^{-1}} \right] \int_v \frac{f_v dv}{[\text{Jy km s}^{-1}]}, \\ &= 2.356 \times 10^5 D^2 10^{17.40 - m_{21,c}}, \end{aligned} \quad (2)$$

where  $D$  is the distance to the galaxy in Mpc, taken from Muñoz-Mateos et al. (2015), and  $m_{21,c}$  is the corrected magnitude of the 21 cm H I line flux from *HyperLeda* (Makarov et al. 2014).

Comerón et al. (2018) derived  $M_{\text{CMC}}$ , of which we avail ourselves, from their SB profile decomposition of S<sup>4</sup>G galaxies. Circular velocity ( $V_{\text{rot}}$ ) data were also taken from the compilation of Comerón et al. (2018). If possible, Comerón et al. (2018) sourced data for the derivation of  $V_{\text{rot}}$  from the Extragalactic Distance Database (EDD; Tully et al. 2009), which provides information and analysis of H I line widths to determine  $V_{\text{rot}}$ . Otherwise, Comerón et al. (2018) sourced  $V_{\text{rot}}$  data from stellar absorption line studies (see Comerón et al. 2018 for a comprehensive list of sources). Fig. 1 shows a comparison of our sub-sample (red histograms) with the full S<sup>4</sup>G sample. Our sub-sample favors slightly more massive, though H I poorer, systems.

Lastly, we consider whether the environments of our sample galaxies may affect their intrinsic flattening as a result of tidal interactions from neighbour galaxies, thus potentially leading to the heating of stellar disks. To investigate this effect, we sourced both the Dahari parameter ( $Q$ ; Dahari 1984) and the projected surface density to the third nearest neighbour galaxy from Laine et al. (2014).

## 4. DATA REDUCTION METHODOLOGY: SURFACE PHOTOMETRY

Our definition of disk intrinsic flattening relies on the ratio of the characteristic radii  $c$  and  $a$ . For an edge-on disk,  $c$  represents the vertical axis above the disk, while  $a$  is the semi-major radius measured at any surface brightness or density. While in principle incorrect for edge-on disks, we have applied elliptical isophote fitting to our galaxy images to extract  $c/a$  at any galactocentric radius<sup>1</sup>.

We have used the Python-based automated light profile extraction tool AutoProf (Stone et al. 2021) to perform image pre-processing and isophotal fitting on each S<sup>4</sup>G sub-sample galaxy image. An image pixel scale of 0.75'' and a zero-point magnitude of 18.32 in the Vega system were used for our S<sup>4</sup>G images. Masks for each galaxy image were retrieved from the S<sup>4</sup>G Pipeline 2 (Sheth et al. 2010; Muñoz-Mateos et al. 2015) and used in AutoProf during processing. Deconvolution of our images with the IRAC 3.6  $\mu\text{m}$  PSF was not necessary, as justified in App. A. As a typical example, Fig. 2 shows the isophotal fit of IC 0335. Our rejection criteria, detailed in Sec. 4.2, resulted in a final sample of 133 galaxies.

### 4.1. Characteristic Cuts

Our measurement of the intrinsic flattening of the stellar disk component used two ensembles of isophotes that span large sections of the disk. The constituent isophotes are those that intersect the galactic midplane within two cuts

<sup>1</sup> A correct measurement of  $c/a$  requires contours of constant density, which cannot be obtained without a full three-dimensional galaxy model as the vertical and axial galactic structures follow different functional forms. Still, our application of selected cuts to edge-on systems provides an operational definition of  $c/a$ .

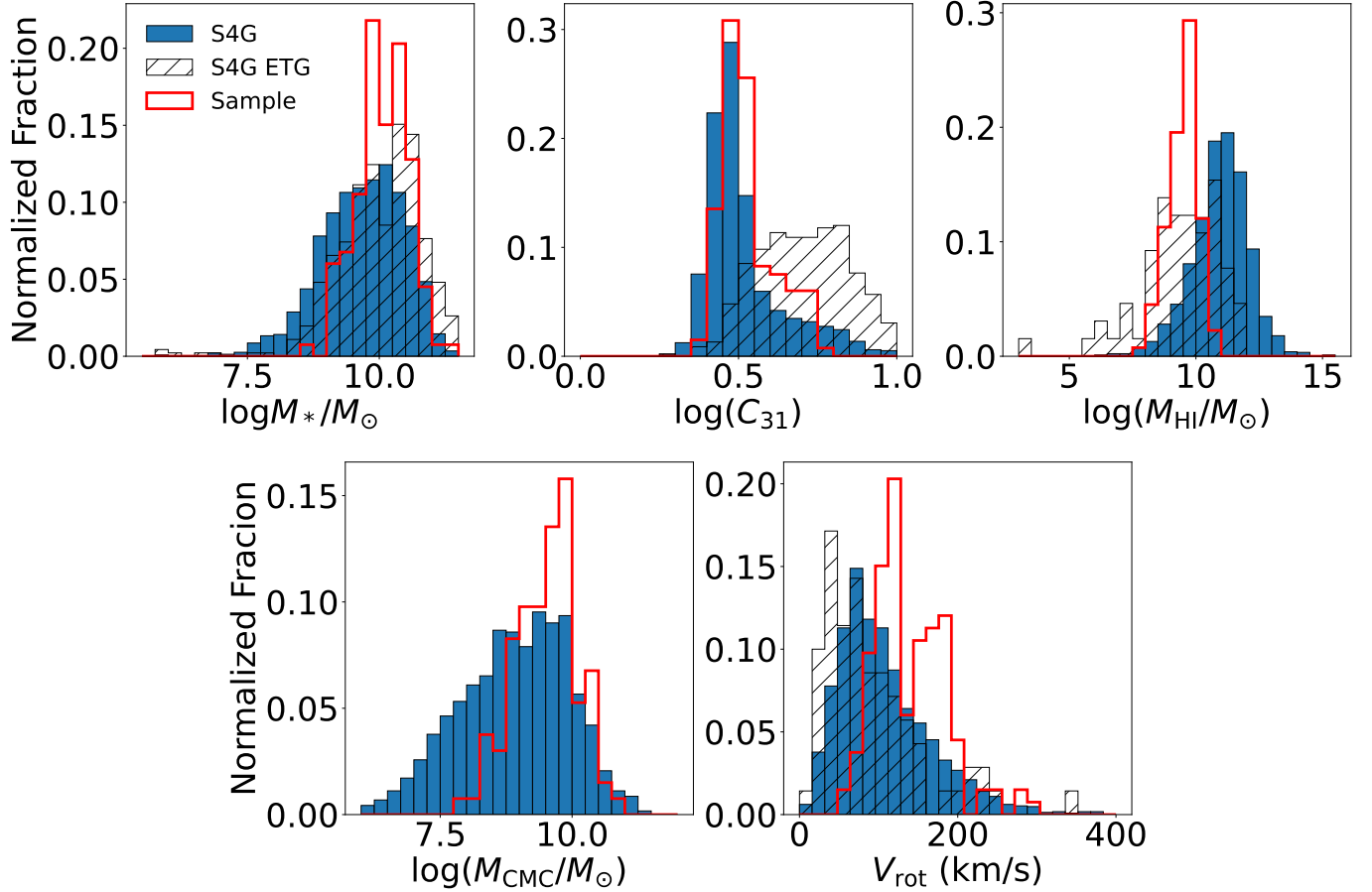


**Figure 1.** Comparison of our sub-sample (red histograms) with the S<sup>4</sup>G catalogue (blue histograms) and (when available) the S<sup>4</sup>G early type galaxy catalogue (hatched histograms).

defined relative to the radius of the 25<sup>th</sup> B-band magnitude isophote,  $r_{25}$ . These cuts, depicted in Fig. 3, are defined by  $0.2r_{25} \leq |a| \leq 0.5r_{25}$ , for the inner cut, and  $0.5r_{25} \leq |a| \leq 0.8r_{25}$ , for the outer cut where  $a$  is the galactocentric radius along the major axis of the galaxy. While this choice is somewhat arbitrary, they match those of Comerón et al. (2018), allowing for direct comparisons. These cuts also roughly divide isophotes dominated by the thin and thick disk light, respectively.

At radii below  $0.2r_{25}$ , rapid variations of  $c/a$  characteristic of the bulge are found. These should not enter our estimates of the intrinsic thickness of the disk. Within the inner cuts between  $0.2$ – $0.5r_{25}$ , a sequence of lowest  $c/a$  for the thin disk is expected, while higher values are expected for the outer cuts for the thick disk between  $0.5$ – $0.8r_{25}$ . At larger radii beyond  $0.8r_{25}$ ,  $c/a$  should converge to any value of  $c/a$  representative of the final galaxy outskirts, possibly affected by flaring or interactions with neighbours. Ideally, our measurements of  $c/a$  ought to be made within the inner cuts as we demonstrate below. Furthermore, concerns about light scattered by PSF wings are alleviated in the inner cuts as these are regions of relatively high surface brightness. For the dimmer outer cuts, scattered light from the midplane was also shown to be small (Comerón et al. 2018).

The mean  $c/a$  of isophotes within both inner and outer cuts is taken to be the intrinsic flattening within the region of the respective cut. The error on this mean is the quadrature sum of the standard deviation of  $c/a$  values within the cut and the uncertainty resulting from the propagation of each individual isophote’s  $c/a$  error through the calculation of the mean. The ellipticity of the isophotes within a given cut varies for all galaxies, so this averaging smooths over any fluctuations in thickness, allowing us to probe the true flattening of the disk. As an example, the top panel of Fig. 3 shows the radial variations of  $c/a$  for the galaxy IC 0335. While no two galaxies have identical radial  $c/a$  profiles, IC 0335 highlights our method’s ability to sample two distinct disk structural regimes. The bottom panel of Fig. 3

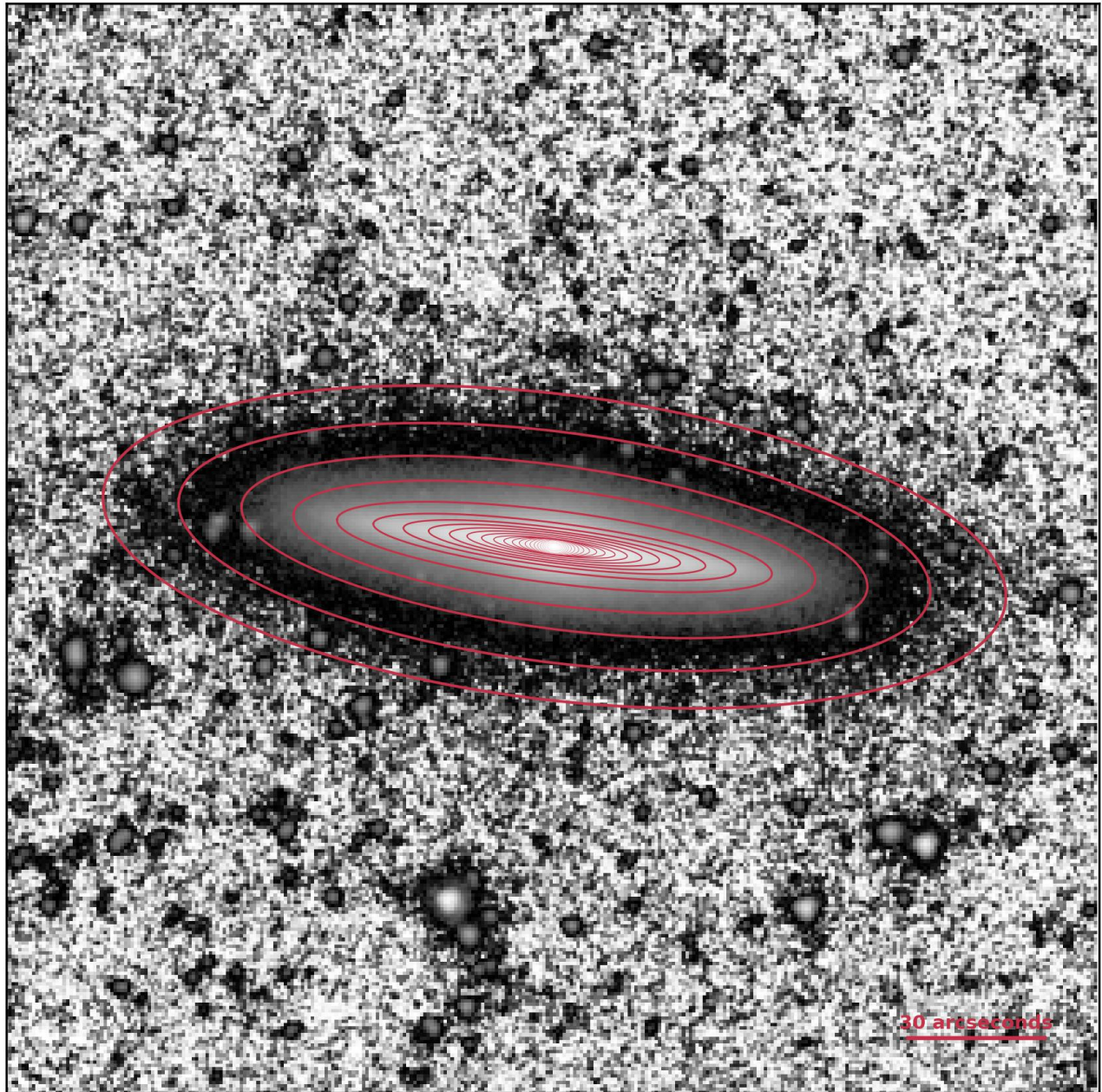


**Figure 2.** Contours of constant surface brightness (isophotes) for the galaxy IC 0335 produced by AutoProf. Every fifth isophote is plotted as a red contour.

presents the density distribution of the  $c/a$  profiles with radius for all 133 galaxies in our sample. Our choice of cuts is meant to separate the CMC and the thin/thick disk components.

We can divide our sample into two global sub-samples: the first consisting of all spiral galaxies, and the second of all lenticular galaxies in our sample. The black line at  $c/a = 0.12$  in the bottom panel of Fig. 3 anticipates results from our analysis of the distribution of  $c/a$  for our spiral sub-sample. This line describes the mean inner cut  $c/a$  of spiral galaxies and highlights that the outer cuts are systematically thicker than the inner cuts, as expected.

#### 4.2. Rejected Isophotal Fits

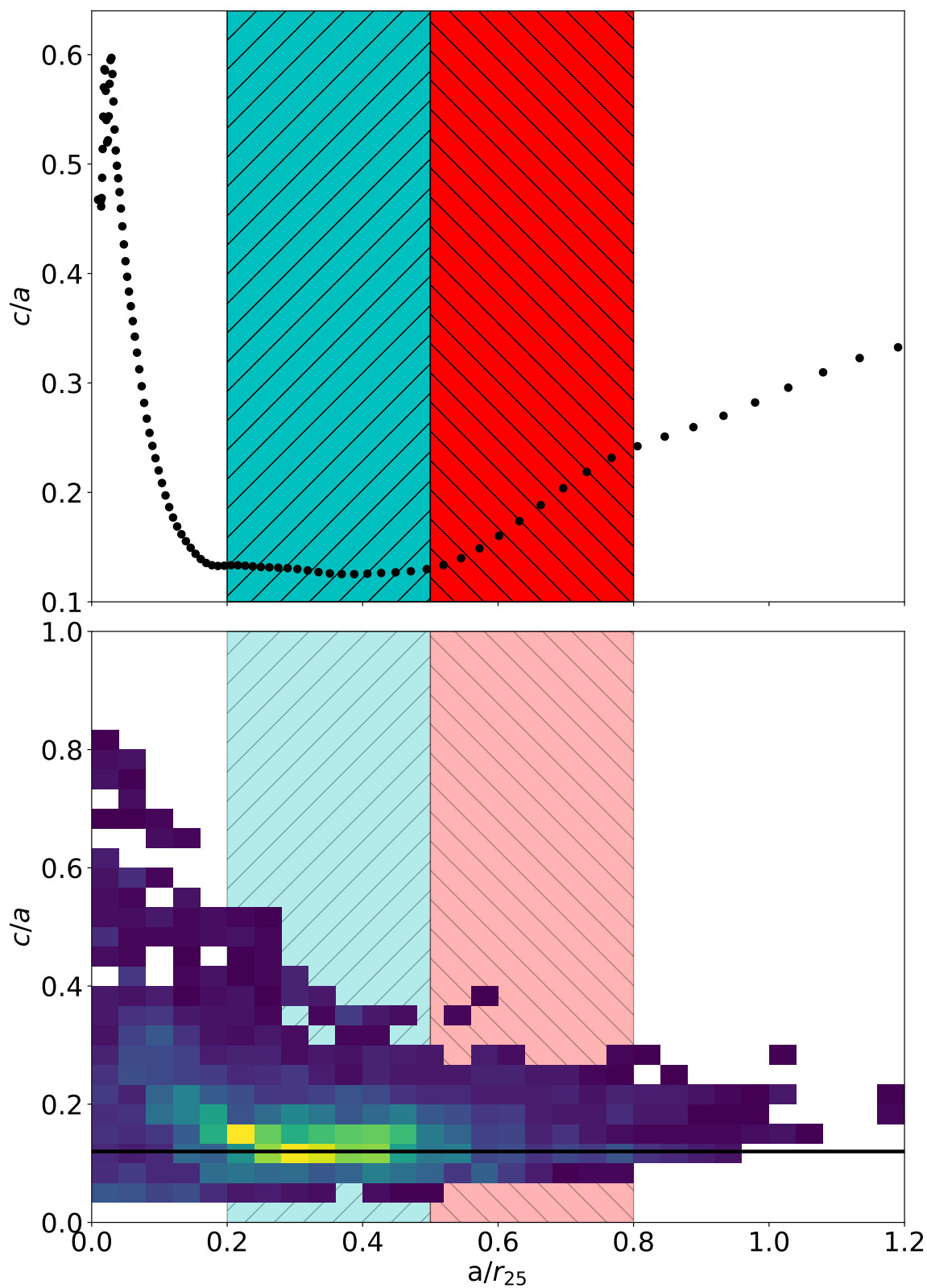


**Figure 3.** Top: Radial profile of intrinsic flattening for IC 0335 (as a typical example). The teal upward hatched area and the red downward hatched area define the inner cut from  $0.2-0.5 a/r_{25}$  and the outer cut over  $0.5-0.8 a/r_{25}$ , respectively. Bottom: Stacked density distribution of all 133 intrinsic flattening radial profiles in our sample. The horizontal black line marks  $c/a = 0.12$ . See text for details.



Despite AutoProf’s robust data reduction, we visually reviewed the resulting isophotal fits to ensure no galaxies with erroneous isophotes entered our analysis. Isophotes in the inner and outer cuts were expected to be well behaved, as in the top panel of Fig. 3. All together, three fits were affected by foreground objects and rejected. AutoProf failed to fit a further five galaxies with masking, yielding a final sample of 133 galaxies.

### 4.3. Statistical Corrections

As a result of our inability to choose the exact viewing angle of objects in the sky, we consider corrections for deviant galaxy orientations within our data set. Sec. 4.3.1 explores reasonable and worst-case scenarios for a galaxy viewed almost edge-on, while Sec. 4.3.2 derives the statistical correction required to account for the random azimuthal rotation of galaxies.

#### 4.3.1. Inclination Effects

In order to observe the true intrinsic flattening of a disk, it must be viewed exactly edge-on at  $i = 90^\circ$ . However, the reported inclinations (from *HyperLeda*) of our sample fall within  $78^\circ \lesssim i \leq 90^\circ$ . These inclinations were derived using Eq. (1) and are therefore biased by previous measurements of intrinsic flattening. Visual inspection (by the main author as well as Comerón et al. 2012, Mosenkov et al. 2015, and Comerón et al. 2018) suggests that the galaxies in our sample are viewed almost perfectly edge-on. We disregarded previously reported inclinations to eliminate any bias. For robust independent measurements of  $c/a$ , we accepted that some disks may be “excessively” thick and trust our visual pattern recognition (e.g., *Galaxy Zoo*, Lintott et al. 2008). We posit that the true inclinations of the galaxies in our sample fall within the range  $85^\circ < i < 90^\circ$ .

In light of this, one may ask to what degree viewing a galactic disk at inclinations less than  $90^\circ$  biases our measurement of  $c/a$ ? Note that a non-zero tilt will always increase the observed thickness,  $q$  in Eq. (1), or equivalently  $c_{\text{obs}}/a_{\text{obs}}$ . In this case, the maximum error will occur at  $i = 85^\circ$ . If we view a transparent disk with  $c/a = 0.13$  at this inclination, then by solving for  $q$  in Eq. (1) we expect to overestimate  $c/a$  by  $\sim 20\%$ . Likewise, a disk with  $c/a = 0.20$  at this inclination will result in an overestimate of  $\sim 8\%$ . So, for measured  $c/a$  values in the expected range, we will, at worst, underestimate the flattening by  $\lesssim 0.02$ .

Since the sample is heavily biased against inclinations that deviate from the true edge-on perspective (Comerón et al. 2018), we expect an overestimated  $c/a$  by  $\sim 1\%$ . In all but the largest measured  $c/a$  values, these overestimates are on the order of the systematic noise. So,  $c/a$  outliers resulting from deviant inclinations are expected to be rare, and measurements are not corrected for this effect. Nevertheless, to minimize the potential effect of a small number of galaxies that deceptively appear to be aligned edge-on, we also used the median statistic of  $c/a$  to minimize the impact of any outliers in our analysis.

#### 4.3.2. Triaxial Variance Effects

Galactic disks in spiral galaxies are triaxial spheroids obeying  $c < b < a$  (rather than  $c < b = a$ ). On average, spiral galaxies are only slightly triaxial, with mean face-on axial ratio  $\langle b/a \rangle = 0.9$  (Lambas et al. 1992). Due to the random orientation of galaxies in the sky, measurements of  $a_{\text{obs}}$  have  $b \leq a_{\text{obs}} \leq a$ . On average, we expect  $\langle a_{\text{obs}} \rangle \simeq 0.97a$ . Therefore, we apply a 3% downward correction to reported mean and median  $c/a$  values. Uncorrected values are denoted by prime indices (e.g.,  $\mu'$ ).

## 5. CHARACTERISING INTRINSIC FLATTENING IN EDGE-ON SYSTEMS

With our measurements of line-of-sight fluxes at well-defined galactocentric locations for 133 S<sup>4</sup>G galaxies, we can establish the distributions of intrinsic flattening,  $c/a$ , for spiral and lenticular galaxies (Sec. 5.1). Their uncertainty-weighted histograms are presented in Fig. 4. We then explore the connection between disk thickness and morphology in Sec. 5.1, and test in Sec. 5.2 for correlations between the physical parameters detailed in Sec. 3.3 and intrinsic flattening. Our  $c/a$  values are also compared to the parametric decompositions of Comerón et al. (2018) in Sec. 5.3. We close this section with an assessment of environmental effects on disk thickness in Sec. 5.4.

### 5.1. The Distribution of Intrinsic Flattening vs Morphology

Our binning of galaxies into lenticular ( $-3 \leq T \leq 0$ ) and spiral ( $1 \leq T \leq 9$ ) morphologies reveals that spirals are well described by a Gaussian distribution for both the inner and outer cuts; see Fig. 4. The outer cut distribution of lenticulars in Fig. 4 is also reasonably Gaussian. The mean and standard deviation of each Gaussian fit are presented in Table 2.

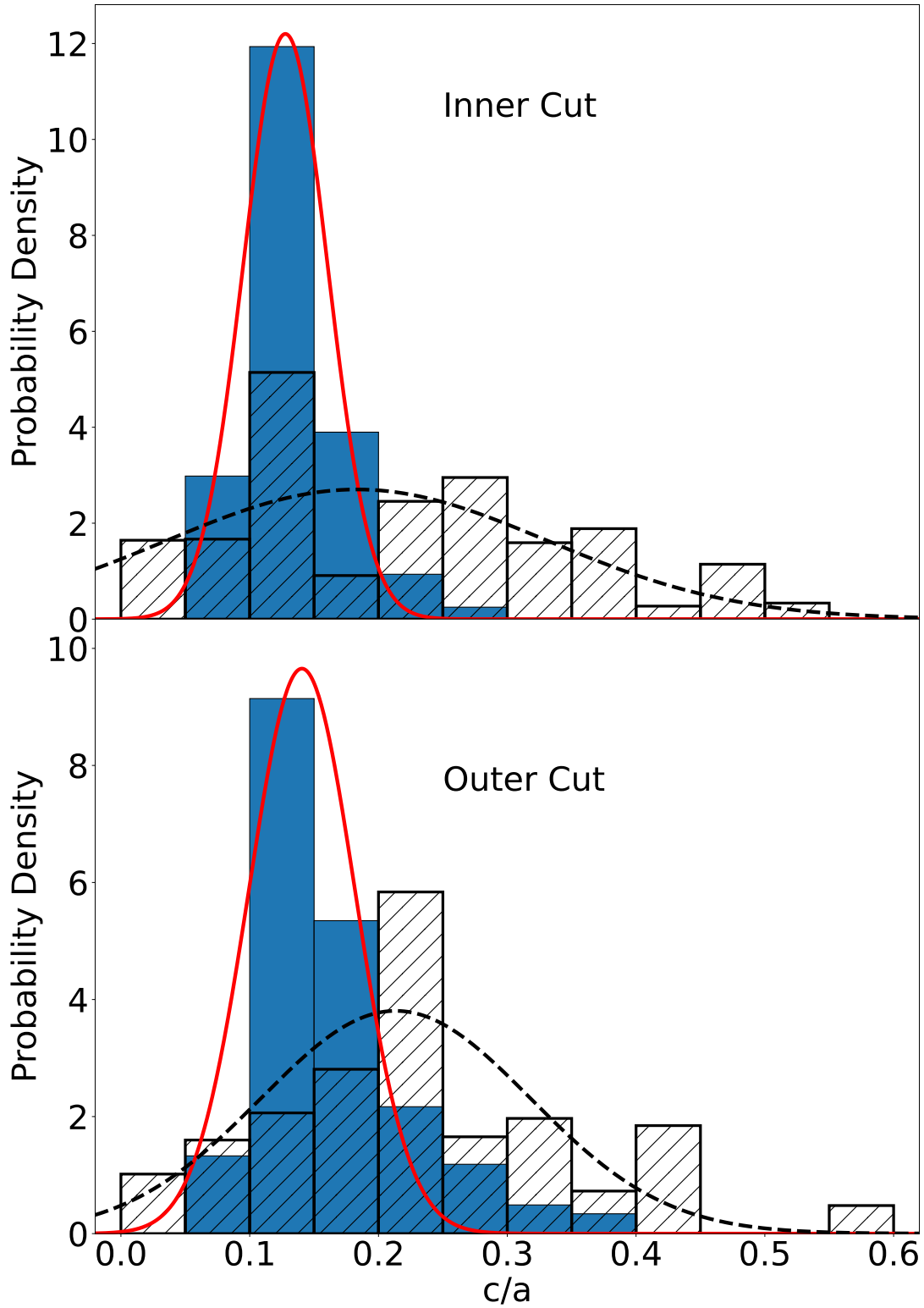


**Figure 4.** Intrinsic flattening distribution of the inner cut (top) and outer cut (bottom). The solid blue and hatched histograms represent spiral and lenticular galaxies, respectively. The solid red and dashed black lines are Gaussian fits to the spiral distributions and the lenticular distributions, respectively.

	Spiral Galaxies		Lenticular Galaxies	
	Inner Cut	Outer Cut	Inner Cut	Outer Cut
$\mu'$	$0.128 \pm 0.001$	$0.140 \pm 0.003$	$0.18 \pm 0.03$	$0.21 \pm 0.02$
$\mu$	$0.124 \pm 0.001$	$0.136 \pm 0.003$	$0.17 \pm 0.03$	$0.20 \pm 0.02$
$\sigma$	$0.033 \pm 0.001$	$0.041 \pm 0.003$	$0.15 \pm 0.02$	$0.10 \pm 0.02$
$m$	0	0	$-0.04 \pm 0.02$	$-0.01 \pm 0.01$
$b$	$0.141 \pm 0.005$	$0.16 \pm 0.01$	$0.18 \pm 0.03$	$0.20 \pm 0.02$

**Table 2.** Top section: Mean and standard deviation of the Gaussian fits performed on the intrinsic flattening distributions of Fig. 4.  $\mu'$  is the mean without accounting for triaxiality (see Sec. 4.3.2), while  $\mu$  includes this correction. Bottom section: Slope,  $m$ , and y-intercept,  $b$ , of the linear fits mapping  $T$  to  $c/a$  (plotted in Fig. 5) with the functional form  $c/a = mT + b$ . The slopes for spiral galaxies are statistically consistent with zero.

Hubble Type	$N^a$	Inner Cut Median $c/a$	Outer Cut Median $c/a$	HG84 $c/a$
-3	7	$0.27 \pm 0.15$	$0.20 \pm 0.16$	0.23
-2	23	$0.28 \pm 0.12$	$0.22 \pm 0.10$	0.23
-1	12	$0.23 \pm 0.11$	$0.21 \pm 0.09$	0.23
0	8	$0.15 \pm 0.17$	$0.18 \pm 0.13$	0.23
1	1	$0.146 \pm 0.003^b$	$0.131 \pm 0.001^b$	0.23
2	5	$0.12 \pm 0.07$	$0.12 \pm 0.10$	0.20
3	4	$0.18 \pm 0.05$	$0.20 \pm 0.06$	0.175
4	7	$0.14 \pm 0.04$	$0.18 \pm 0.05$	0.14
5	13	$0.14 \pm 0.04$	$0.13 \pm 0.04$	0.103
6	14	$0.13 \pm 0.02$	$0.14 \pm 0.04$	0.10
7	27	$0.14 \pm 0.04$	$0.17 \pm 0.07$	0.10
8	7	$0.12 \pm 0.04$	$0.14 \pm 0.05$	0.10
9	5	$0.15 \pm 0.04$	$0.19 \pm 0.05$	0.10

**Table 3.** Median intrinsic flattening values for the inner and outer cuts versus Hubble Type  $T$ . The reported errors are the standard deviations of the mean.  $a$  - Number of galaxies.  $b$  - The uncertainty is a result of a singular data point and is grossly underestimated. The last column shows the  $c/a$  values reported in HG84.

The spiral galaxies follow relatively tight  $c/a$  distributions in both cuts, the narrowest width being achieved for the inner cuts. For the inner cuts of spiral galaxies in our sample, we find  $\langle c/a \rangle = 0.124 \pm 0.033$ . This value for the intrinsic flattening agrees well with Guthrie (1992) and Giovanelli et al. (1994).

A small tail extending to a flattening of 0.4 exists in the outer cut spiral distribution. Since this tail is not present in the spiral's inner cut distribution, it is unlikely to be an artifact of either inclination or triaxiality effects. Rather, as discussed in Sec. 4.1, this tail likely arises from slight luminous contributions from non thin-disk sources such as a thick disk, disk flaring, nearby objects, or even light scattered by the PSF (Sandin 2014, 2015).

For lenticular galaxies, the  $c/a$  means for the inner and outer cuts (see Table 2, as well as both panels of Fig. 4) agree, while the deviations do not. Both values are notably larger than their spiral counterparts. This is a clear reflection of their more troubled past relative to much thinner spiral galaxies (see below).

We report the median intrinsic flattening for each Hubble Type in Table 3, along with the  $c/a$  values reprinted in HG84 for the corresponding  $T$ . The individual data used to assemble Table 3 are also plotted in Fig. 5, where the  $c/a$  value of each galaxy is shown versus the galaxy's Hubble Type. Measurements for each galaxy are marked as red  $x$ 's in this figure. The median  $c/a$  values reported in Table 3 are also plotted as black points with error bars that denote the scatter of  $c/a$  for a given  $T$ . Panels a), c), and e) show the inner cut  $c/a$  values, while b), d), and f) use outer cut values.

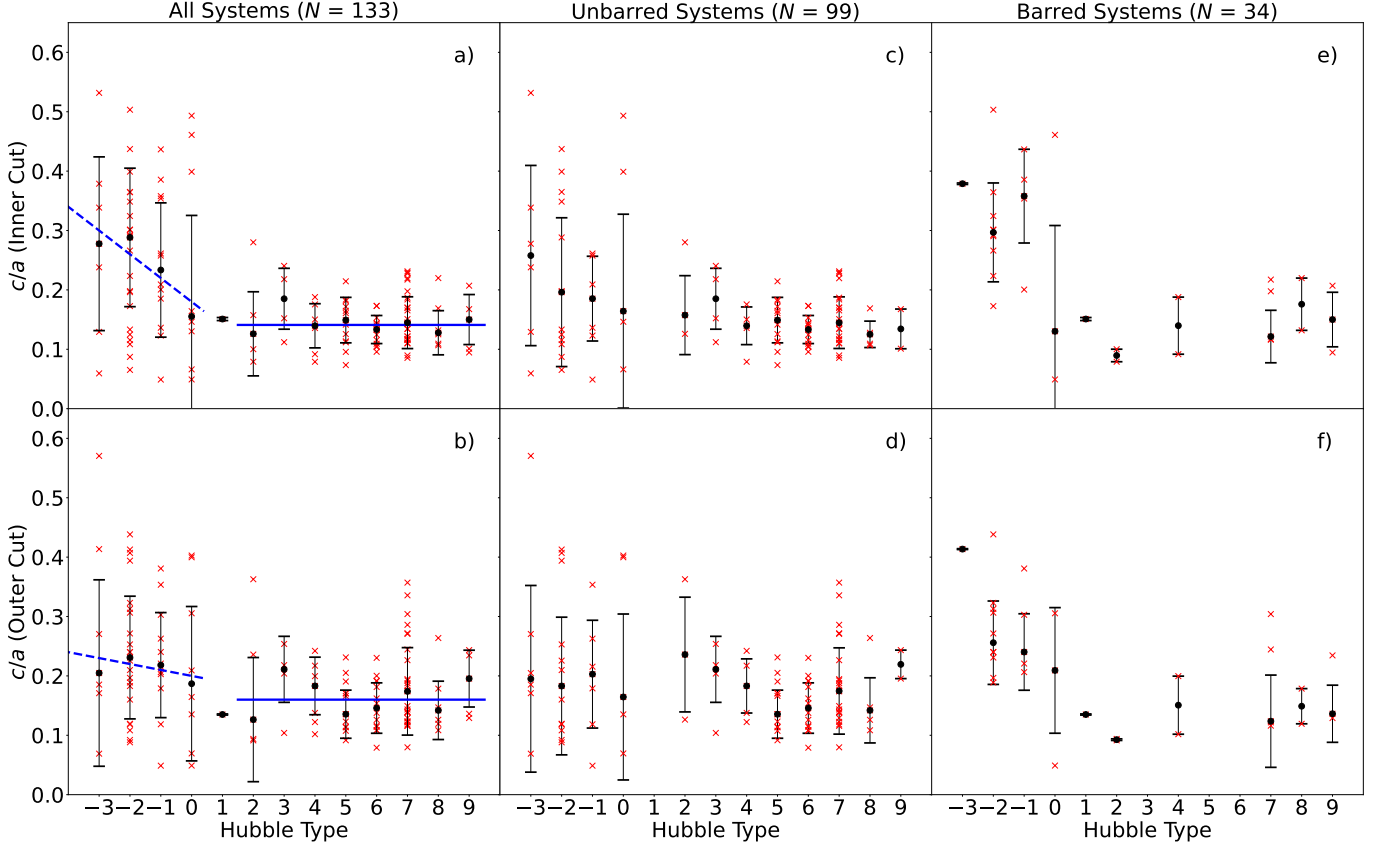


**Figure 5.** Intrinsic flattening of disk galaxies by Hubble Type based on the inner (top) and outer (bottom) cuts. Black points are the median  $c/a$  values for each Hubble Type, while error bars represent the dispersion. Red  $x$ s are  $c/a$  values for individual galaxies. Error bars on the individual galaxy points have been omitted for the sake of clarity and are on the order of 1-2%. In panels a)-b), each solid blue line is a linear fit to the median flattening of disk galaxies ranging from  $T = 2$  to  $T = 9$ , while each dashed blue line is a linear fit to the lenticular galaxies median  $c/a$ . In panels c)-f), unbarred and barred systems are shown separately without fits for visual comparison with the full set. The  $c/a$  distributions for barred and unbarred disk galaxies are comparable.

For lenticular galaxies ( $T = [-3, 0]$ ), we find that earlier systems appear to be thicker, albeit with large scatter, in agreement with older findings (Binney & de Vaucouleurs 1981). The thickening towards earlier types can be attributed to the evolutionary processes that shaped them; galaxy interactions increase the velocity dispersion in the disk while gas depletion halts the formation of new, low velocity dispersion stars (Comerón et al. 2016; Pinna et al. 2019a,b). Our result above contrasts with HG84’s constant intrinsic flattening ( $c/a = 0.23$ ) for all lenticulars.

For the later-type disks ( $T = [2, 9]$ ), the median thickness is mostly constant with  $c/a \simeq 0.14$ . This result holds within uncertainties for either inner or outer cuts. HG84 also quoted a nearly constant flattening for  $T = [5, 9]$  disk galaxies, albeit with a smaller amplitude ( $c/a \simeq 0.10$ ). We find no evidence of the disk thickening reported by HG84 from  $T = 5$  to  $T = 1$ , though our counts for these types are low.

Panels a) and b) of Fig. 5 show linear fits to the lenticular and  $T > 1$  spiral  $c/a$  values. These fits are parameterised in Table 2.  $T = 1$  has been excluded from the spiral fits given the bin consists of one object. The slopes of the spiral galaxy fits are statistically consistent with, and here fixed to, zero.

We further divided our sample into galaxies visually identified as tentatively hosting a bar or not. The inner and outer cut  $c/a$  values for unbarred galaxies are plotted against  $T$  in panels c) and d) of Fig. 5, respectively. Given the prevalence of barred systems in local spiral galaxies (e.g., Buta et al. 2015; Vera et al. 2016; Vázquez-Mata et al. 2022), many bars have likely been missed due to the restricted edge-on views. Panels c) and d) of Fig. 5 may therefore include a large number of unidentified barred galaxies. Still, based on the available information and given the caveats noted above, no marked difference in the intrinsic flattening of barred vs unbarred galaxies is noticed.

	$N$	Inner Cut		Outer Cut	
		$r_p$	$p$	$r_p$	$p$
$\log M_*/M_\odot$	133	0.14	<b>10%</b>	0.01	<b>87%</b>
$\log C_{31}$	133	0.71	$\ll 1\%$	0.49	$\ll 1\%$
$\log M_{\text{HI}}/M_\odot$	106	-0.13	<b>19%</b>	-0.17	<b>8%</b>
$\log M_{\text{CMC}}/M_\odot$	75	0.45	$\ll 1\%$	0.31	0.6%
$V_{\text{rot}}$	133	0.03	<b>77%</b>	-0.14	<b>9%</b>

**Table 4.** Pearson correlation coefficients and their significance for the correlations between  $c/a$  and the physical parameters plotted in Fig. 6.  $N$  is the number of galaxies for which the relevant parameter exists.  $r_p$  is the Pearson correlation coefficient.  $p$  is the two-sided  $p$ -value that denotes the significance of the correlation.

### 5.2. Intrinsic Flattening and Other Structural Parameters

We now investigate potential correlations between intrinsic flattening and other physical parameters listed in Sec. 3.3. Note that not all galaxies have recorded values for each parameter. Fig. 6 shows those correlations with squares and circles denoting lenticulars and spiral galaxies, respectively. The shade of coloured labels identifies the Hubble Type.  $T = 0$  galaxies are grey squares. The Pearson correlation coefficients for each relation shown in Fig. 6 are presented in Table 4. A few significant correlations with  $c/a$  can be gleaned from Fig. 6, while most of the tested variables such as stellar mass, HI mass, and circular velocity, show no correlation. In the next section, we examine the surprising lack of correlation between  $c/a$  and  $V_{\text{rot}}$  in the context of parametric decompositions.

The light concentration index,  $C_{31}$ , seems to correlate fairly well with  $c/a$  for the inner cut ( $r_p = 0.71$ ), as quantified in Table 4. The spiral and lenticular galaxies seem to form a global  $c/a - \log C_{31}$  trend. Closer investigation of this trend reveals that it is entirely supported by the lenticulars, while the spirals show no correlation<sup>2</sup>. Such a trend should also appear between  $\log M_{\text{CMC}}$  and  $c/a$ , but is surprisingly absent. The  $\log M_{\text{CMC}} - c/a$  relations in panels g) and h) of Fig. 6 reveal boundaries defined by the least massive CMCs at any given  $c/a$ . The spirals have a sharply rising lower bound on  $M_{\text{CMC}}$ , while the lenticulars have central mass concentrations more massive than  $10^9 M_\odot$ , regardless of  $c/a$ .

Despite the lack of correlation of  $c/a$  with many variables, similar boundaries stand out in the other panels of Fig. 6. For instance, panels a) and b) suggest a boundary for the minimum total stellar mass as a function of  $c/a$ . For spirals, that boundary grows as the disk thickens (growing  $c/a$ ), while lenticulars are limited to  $\log(M_*/M_\odot) \geq 9.8$ . Similar boundaries are present in the other panels for spiral galaxies.

The boundaries in panels a), b), g) and h) of Fig. 6 for lenticular galaxies are largely driven by selection biases stemming from our requirement for highly inclined galaxies; bulges must be massive for their host to be identified as a lenticular in the edge-on perspective. The S<sup>4</sup>G includes lenticulars with stellar masses down to about  $10^8 M_\odot$  (Watkins et al. 2022), confirming that our sample is deficient in lenticulars with stellar masses below  $\sim 10^{9.8} M_\odot$ . It is therefore likely that the trend seen in the  $\log C_{31} - c/a$  relation established by lenticular galaxies is mostly a result of selection.

### 5.3. Correlations between $c/a$ and Model-Dependent Parameters

Parametric decompositions of galaxies have become ubiquitous in studies of vertical disk structure (e.g., Gilmore & Reid 1983; Tikhonov & Galazutdinova 2005; Yoachim & Dalcanton 2006; Comerón et al. 2011a,b,c, 2012; Erwin 2015; Comerón et al. 2018). We now test whether parametric and non-parametric measures of disk thickness map into one another. As stated above, relevant model parameters include scale heights,  $z_0$ , of the thin and thick disks, here taken from the SB profile decompositions of Comerón et al. (2018). We have also extracted a global scale length from our own exponential fits to the disk-dominated SB profiles of our S<sup>4</sup>G galaxies, since the scale lengths of Comerón et al. (2018) may correspond to non-disk structures. With these values, we can test for any correlations between  $c/a$  and  $z_0/h$  (Fig. 7), as well as between  $h$  and  $a$  (Fig. 9), and  $z_0$  and  $c$  (Fig. 8).

<sup>2</sup> Caution is advised in interpreting any trend between  $c/a$  and  $\log C_{31}$  if the missing low values of  $C_{31}$  at high  $c/a$  for the lenticulars are due to selection effects.

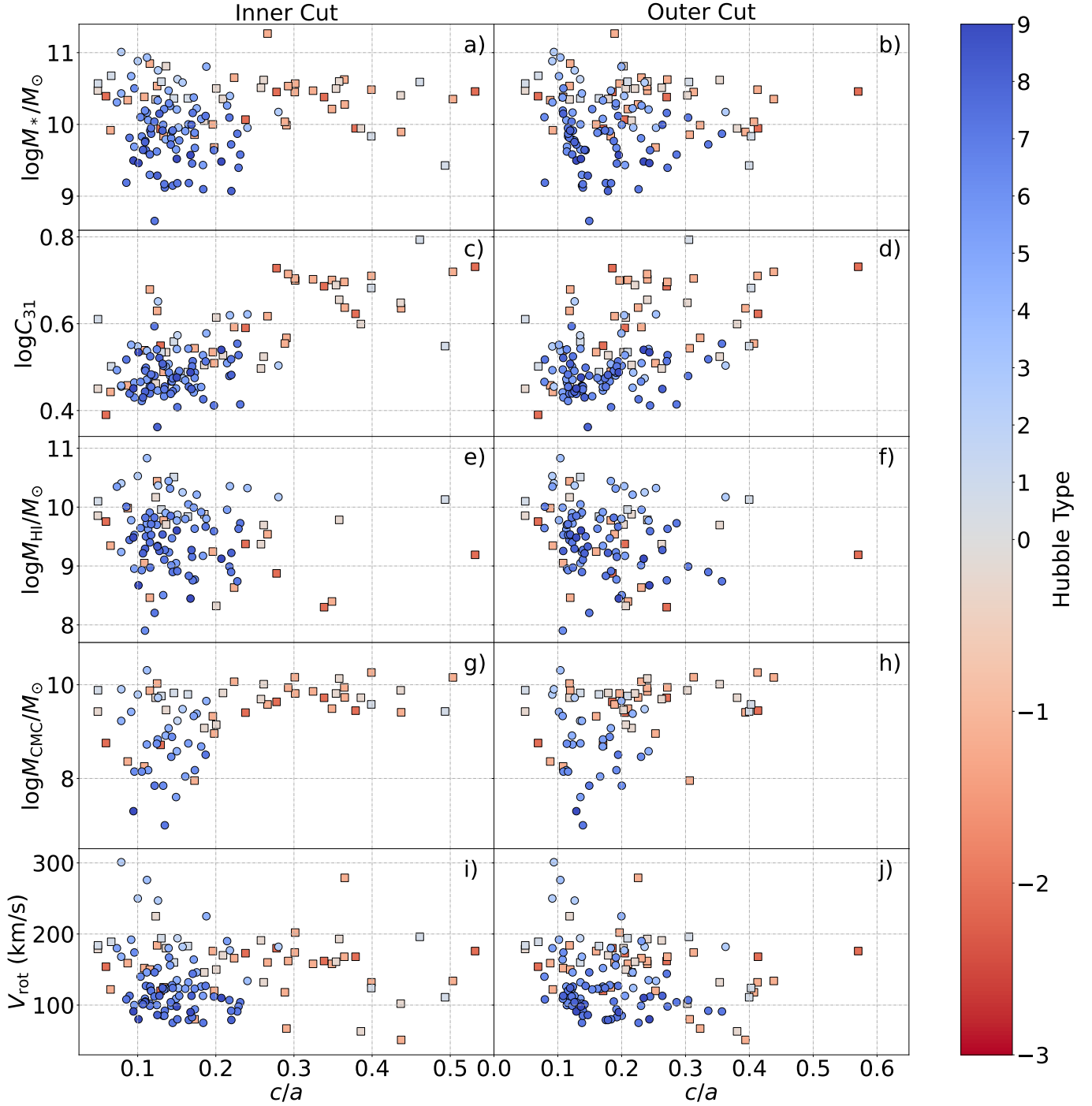


**Figure 6.** Various physical parameters plotted against intrinsic flattening  $c/a$ . From top to bottom, the physical parameters are; total stellar mass; concentration parameter,  $C_{31}$ ; total H I mass; CMC mass; and circular velocity. The left and right columns use the intrinsic flattening of the inner and outer cuts, respectively. Squares and circles represent lenticular and spiral galaxies, respectively. Colours scale with the Hubble Type of the galaxy.

To investigate these trends, we have computed the average value of  $a$  for both inner and outer cuts as  $a_{\text{in}} = 0.35 r_{25}$  and  $a_{\text{out}} = 0.65 r_{25}$ , respectively. To estimate the error on these values, we assigned both values of  $a$  the maximum possible uncertainty of  $a_{\text{err}} = 0.15 r_{25}$ , which is the distance from the center to the edge of either cut. As a result of this choice, the percent errors on  $a$  will be identical for a given cut: 42% error for the inner cut and 23% error for the outer cut. It follows that the semi-minor axis of the characteristic cut is  $c_i = a_i(c/a)_i$ , where  $i$  denotes either the inner

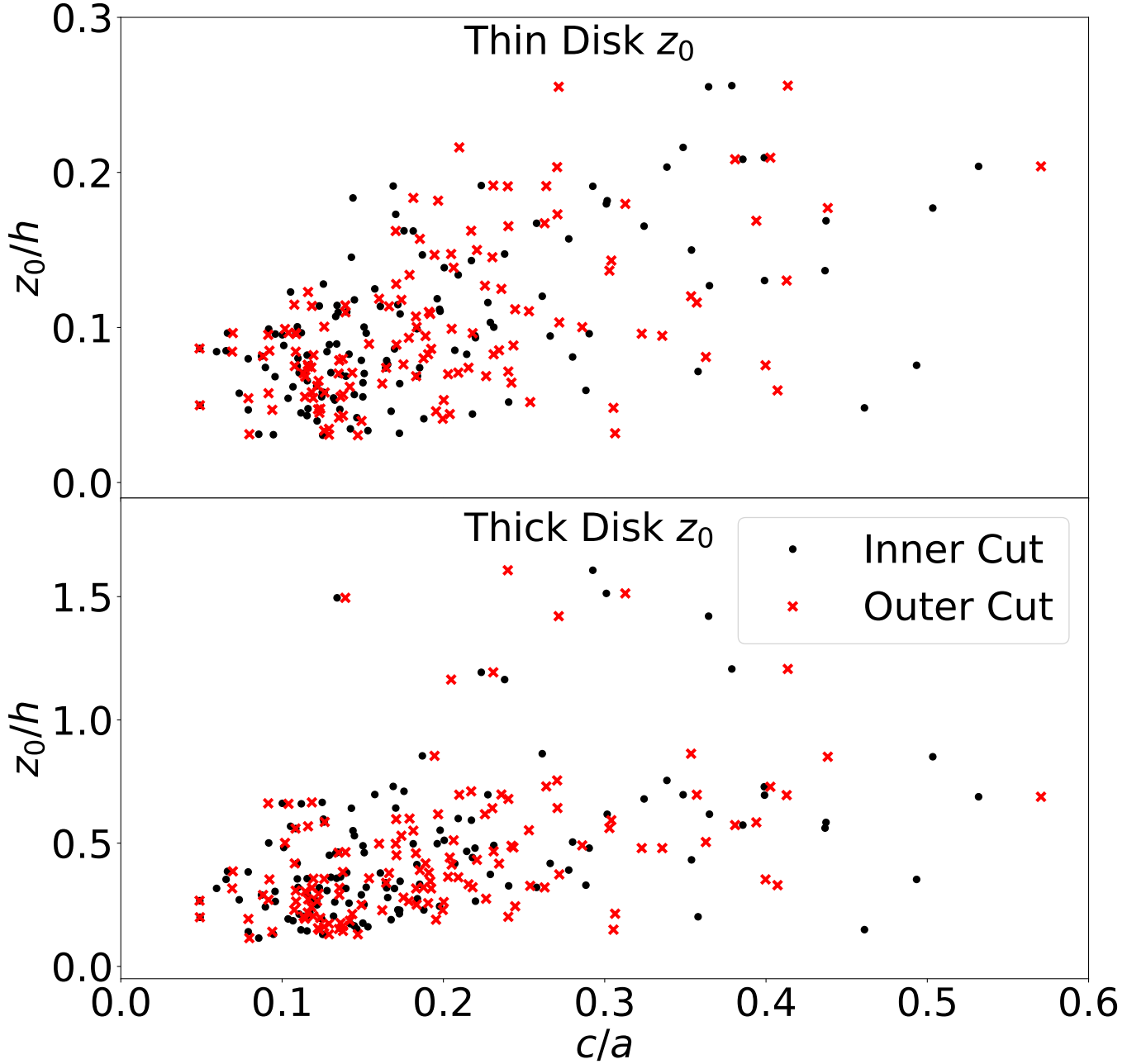


**Figure 7.** Ratio of scale height to scale length plotted against intrinsic flattening,  $c/a$ . Top/Bottom panel: thin/thick disk scale height. Black/red dots indicate intrinsic flattening values derived from inner/outer cuts. Note the different Y-axis limits in both figures.

or outer cut. The uncertainty on  $c/a$  and  $a$  is propagated through to  $c$ . With values of  $a$  in place, values of  $c$  emerge directly from the ratio  $c/a$ .

Weak correlations between  $z_0/h$  and  $c/a$ , as supported by the Pearson correlation coefficients reported in Table 5, are found in Fig. 7. Somewhat stronger correlations ( $r_p \geq 0.7$ ) exist between  $z_0$  and  $c$  as well as  $h$  and  $a$ , as seen in Fig. 8 and Fig. 9, respectively. These suggest that our method and choice of cuts are indeed probing disk structure and properly avoiding the CMC.

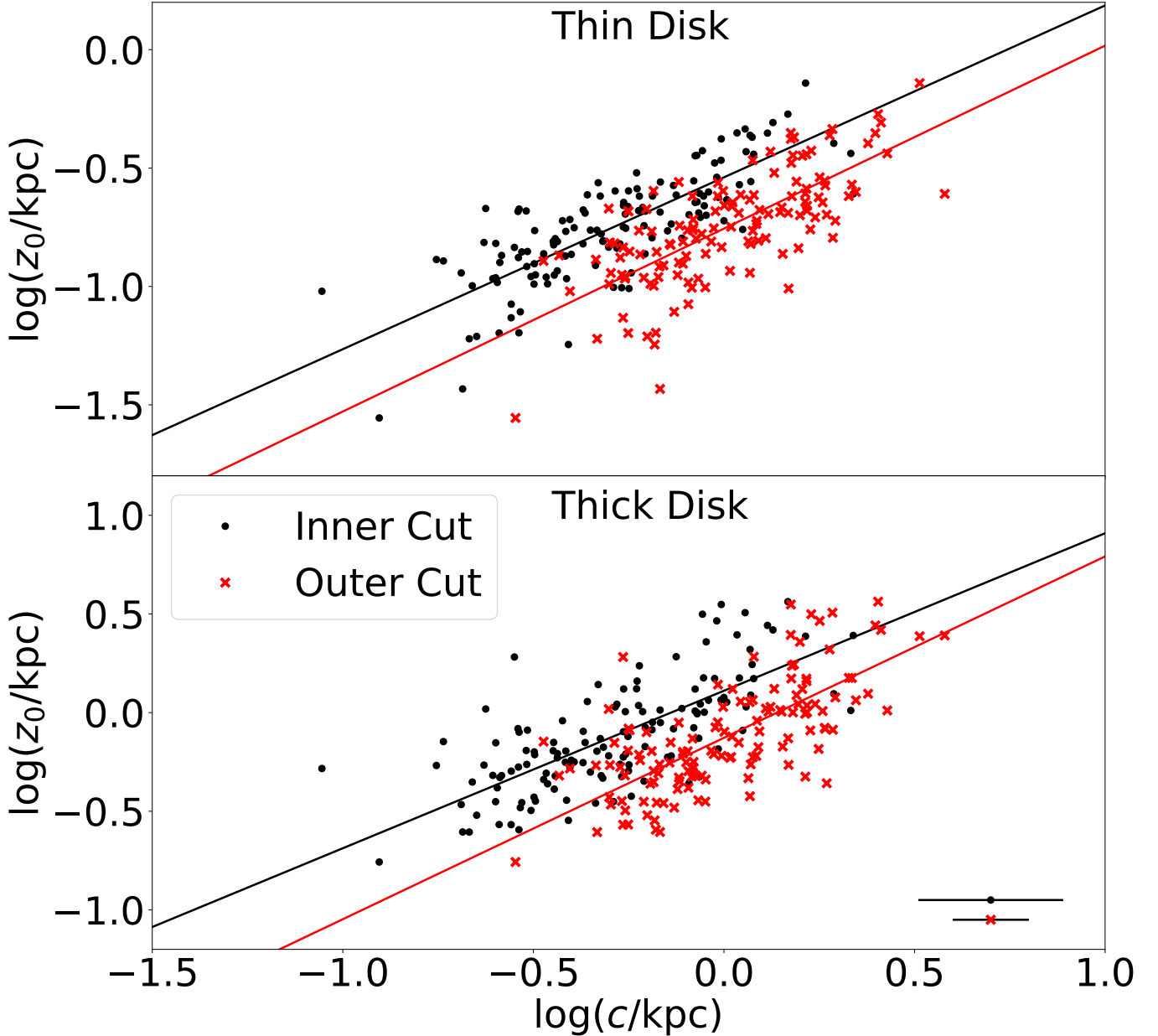


**Figure 8.** Disk scale height versus characteristic cut’s semi-minor axis. Top/bottom panels show thin/thick disk scale height. Black/red dots indicate intrinsic flattening values derived from inner/outer cuts. The solid black/red line is a linear fit to these data.

The thin disk correlations in Table 5 are weaker for the thick disk, likely as a result of a combination of lower S/N in the fainter regions and heightened sensitivity to perturbations in the outskirts. The  $\log h - \log a$  relation is an exception, as the definition of  $a$  and choice of global  $h$  force identical scatters between the inner and outer cuts.

Overall, while some tentative trends ( $r_p \geq 0.7$ ) between  $z_0$  and  $c$ , as well as between  $h$  and  $a$ , exist and are indeed expected on the basis of simple galactic models, a more complex, likely multi-dimensional, analysis of all the galaxy structural variables at play would be required to achieve a closer mapping between parametric and non-parametric tracers of disk thickness. As we shall see in Sec. 6.3, the ratio  $c/a$  remains a better tracer of galaxy disk thickness than  $z_0/h$ .

We close this sub-section by revisiting the (non-)correlation of flattening parameter with  $V_{\text{rot}}$  seen in Sec. 5.2 (Fig. 6, panel (i)). The latter is surprising as one would expect the depth of the potential and magnitude of rotational support



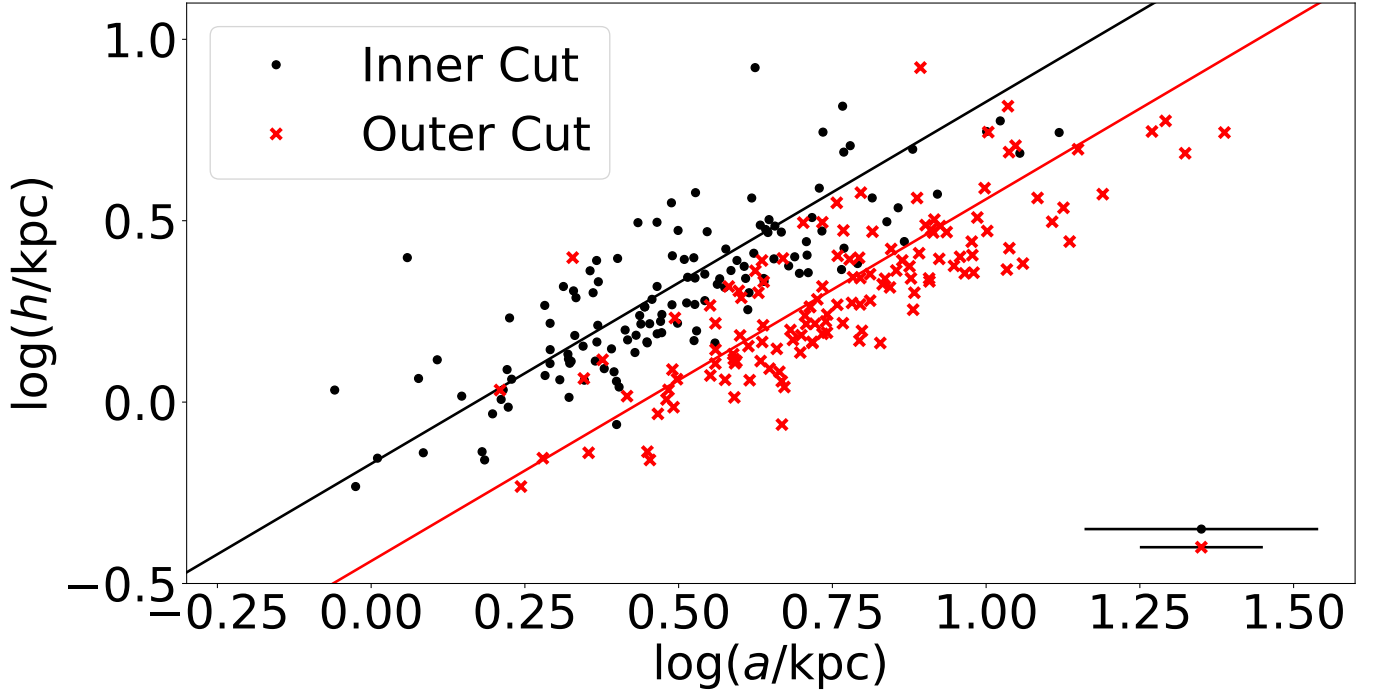


**Figure 9.** Disk scale length versus characteristic cut’s semi-major axis. The scale lengths represent the global disk, not a thin/thick disk decomposition. Black/red dots represent intrinsic flattening values derived from inner/outer cuts. The solid black/red line is a linear fit to these data.

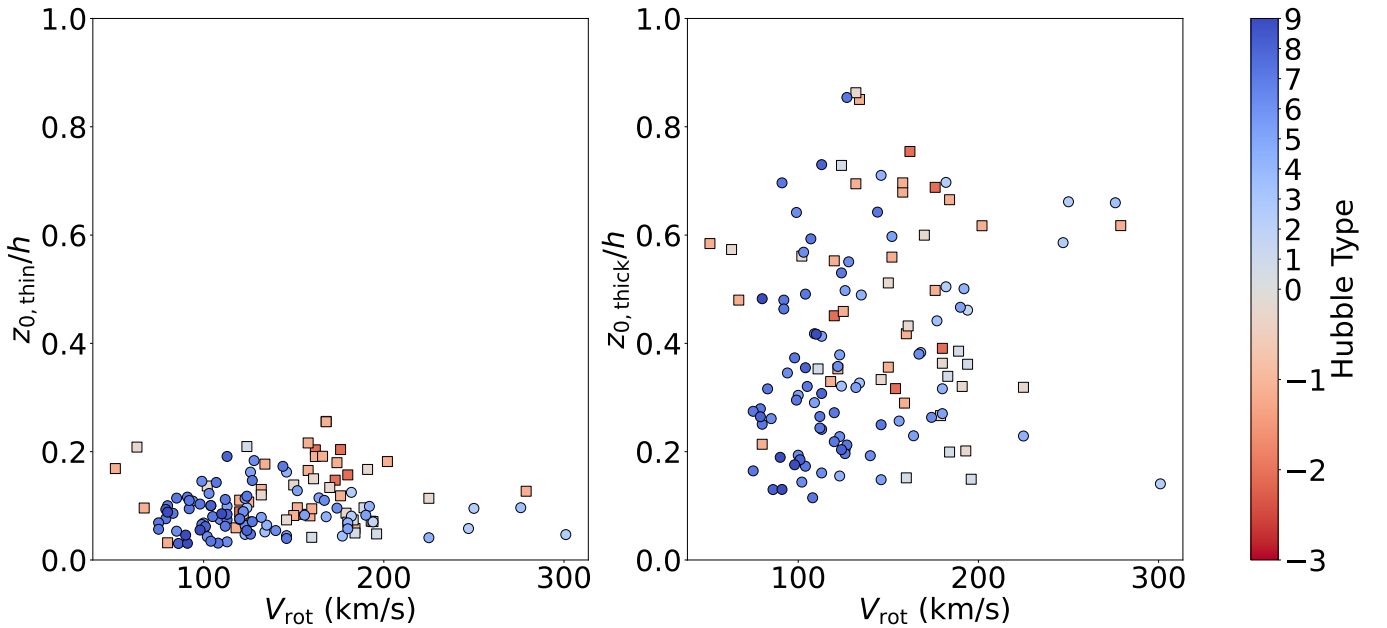


**Figure 10.** Measure of parametric flattening for the thin (left panel) and thick (right panel) disks of spiral and lenticular galaxies versus total rotational speed,  $V_{\text{rot}}$ . In both cases, no correlation between  $z_{0,\text{thin}}/h$  and  $V_{\text{rot}}$  is found. For the thin disks of spiral galaxies (blue circles in the left panel), the mean  $z_{0,\text{thin}}/h = 0.12$  is shown as a thick line. Symbols and colours are as in Fig. 6.

		$z_0/h = m(c/a) + b$			
		Thin Disk		Thick Disk	
		Inner Cut	Outer Cut	Inner Cut	Outer Cut
$m$		0.28	0.28	1.2	1.3
$\Delta m$		0.03	0.04	0.2	0.2
$b$		0.05	0.05	0.23	0.19
$\Delta b$		0.01	0.01	0.05	0.05
$r_p$		0.57	0.52	0.42	0.42
$p$		$\ll 1\%$	$\ll 1\%$	$\ll 1\%$	$\ll 1\%$
		$\log z_0 = m \log c + b$			
		Thin Disk		Thick Disk	
		Inner Cut	Outer Cut	Inner Cut	Outer Cut
$m$		0.72	0.77	0.80	0.92
$\Delta m$		0.05	0.06	0.07	0.08
$b$		-0.54	-0.76	0.11	-0.13
$\Delta b$		0.02	0.01	0.03	0.02
$r_p$		0.78	0.71	0.71	0.70
$p$		$\ll 1\%$	$\ll 1\%$	$\ll 1\%$	$\ll 1\%$
		$\log h = m \log a + b$			
		Inner Cut	Outer Cut		
$m$		1.00	1.00		
$\Delta m$		0.06	0.06		
$b$		-0.17	-0.44		
$\Delta b$		0.03	0.04		
$r_p$		0.81	0.81		
$p$		$\ll 1\%$	$\ll 1\%$		

**Table 5.** The fit parameters for the linear functions  $\frac{z_0}{h}(c/a)$  (top third), and power laws  $z_0(c)$  (middle third), and  $h(a)$  (bottom third). Fit parameters are the slope  $m$  and y-intercept  $b$ , along with their respective errors  $\Delta m$  and  $\Delta b$ .  $r_p$  is the Pearson correlation coefficient of the data.  $p$  is the two-sided p-value that denotes the significance of the correlation.

to affect the stellar disk thickness (e.g., de Grijs et al. 1997; Kregel et al. 2002; Pohlen et al. 2004), as it does with dusty disks (e.g., Dalcanton et al. 2004; Mosenkov et al. 2022). We can here revisit the  $c/a$  vs  $V_{\text{rot}}$  relation in terms of the flattening parametric  $z_0/h$  in order to compare with the references above. This is shown in Fig. 10. Values of  $z_0$  for the thin and thick disks are still from Comerón et al. (2018). While the data in Kregel et al. (2002) agree with ours (Fig. 10), our interpretations for a putative trend between  $z/h$  (or in our case  $c/a$ ) and  $V_{\text{rot}}$  differ, owing in part to our larger data base. Our tests with bona fide  $z_0/h$ , or  $c/a$ , versus  $V_{\text{rot}}$  yield the same conclusion: there is no dependence of  $V_{\text{rot}}$  on disk flattening.

#### 5.4. Galactic Environments

The shapes of S<sup>4</sup>G galaxies could be affected by environmental effects, such as tidal interactions from neighbour galaxies. We used the environmental quantifiers described in Sec. 3.3 to test for correlations between these parameters and intrinsic flattening. Any correlation could suggest whether galactic environments play a key role in driving disk thickness, which would need to be accounted for when deriving the intrinsic  $c/a$ .

However, the top panel of Fig. 11 shows that the Dahari parameter is not correlated with intrinsic flattening (see Table 6.) Although some notably large  $Q$  values indicate the presence of significant tidal forces, the stellar disks of the galaxies experiencing such forces seem neither unusually thick nor thin.

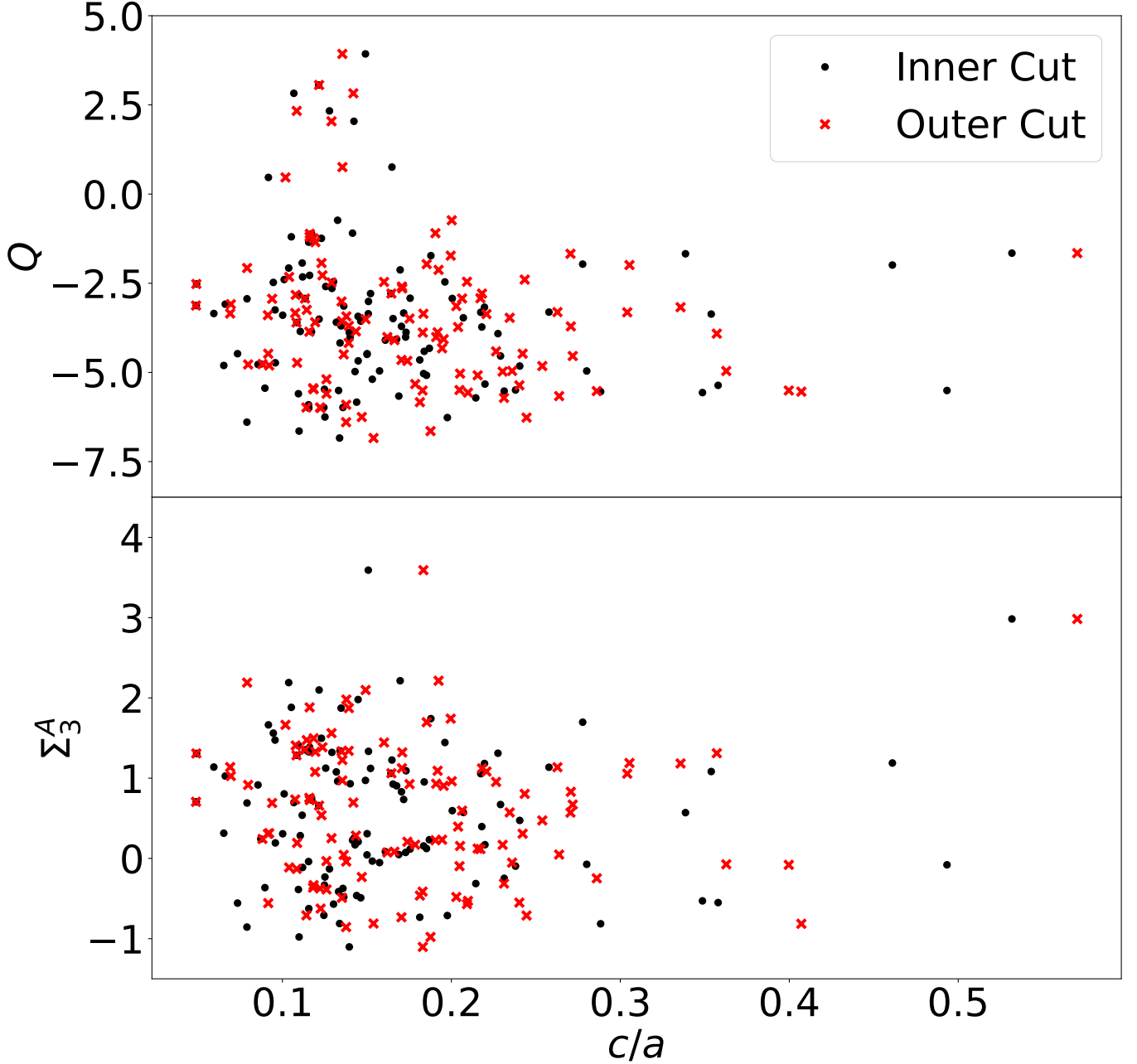


**Figure 11.** Top: Dahari parameter of each galaxy against its inner (blue) and outer (black) intrinsic flattening. Bottom: projected surface density of galaxies to the third nearest neighbour for each galaxy against its inner (blue) and outer (black) intrinsic flattening.

	Inner Cut		Outer Cut	
	$r_p$	$p$	$r_p$	$p$
$Q$	-0.09	<b>36%</b>	-0.16	<b>9%</b>
$\Sigma_3^A$	0.03	<b>72%</b>	-0.01	<b>95%</b>

**Table 6.** Pearson correlation coefficients and their significance for the correlation between environment tracers plotted in Fig. 11 and intrinsic flattening.  $r_p$  is the Pearson correlation coefficient.  $p$  is the two-sided p-value that denotes the significance of the correlation. Boldface p-values are those that fail the significance test.

The bottom panel of Fig. 11 shows an equally large scatter. As reported in Table 6, the surface density of the galaxy group hosting the subject does not correlate with intrinsic flattening. There are two outlying galaxies of interest with large group surface densities. The first, at  $0.1 \leq c/a \leq 0.2$ , does not boast an abnormal intrinsic flattening. Therefore, we do not expect this galaxy’s disk to be biased by its environment. The second outlier lies at  $0.5 \leq c/a \leq 0.6$  in both cuts. The dense environment of this galaxy may be causing the disk to thicken.

Overall, the lack of correlation between our environmental quantifiers suggests that our sample is not affected by close interactions between galaxies.

## 6. DISCUSSION

In Sec. 5, we computed and reported several measurements of  $c/a$  for spiral and lenticular galaxies in Table 2. We further subdivided these samples and reported the median  $c/a$  of each morphological type in Table 3. In what follows, we identify the most reliable  $c/a$  based on our method of characteristic cuts. We further cement these results with a comparative analysis of the parametric  $z_0/h$  in Sec. 6.3.

### 6.1. *The Intrinsic Flattening of Stellar Disks*

We presented in Sec. 5.1 three distinct measures of  $c/a$  for spiral and lenticular galaxies, each applied to the inner and outer cuts (both representing the thin and thick disks) of our galaxy sample. Those measurements of  $c/a$  were: (i) the Gaussian mean of the  $c/a$  distribution (see Fig. 4); (ii) the median  $c/a$  for each Hubble Type, tabulated in Table 3 and plotted in Fig. 5; and (iii) the average of these median  $c/a$  values for spiral morphologies, visualized as the horizontal lines in Fig. 5. The variance in Fig. 4 and Fig. 5 made clear that a global  $c/a$  cannot be reasonably ascribed to lenticular galaxies. Even when binned by Hubble Type, the large scatter persists. It follows that a single estimate for the intrinsic flattening of lenticular systems is not realistic.

For disk galaxies, the tight scatter of the distributions of Fig. 4 makes the results from our Gaussian fits more compelling than the median  $c/a$  values for each spiral morphology in Table 3 due to the larger uncertainties and under-sampled bins of the latter. Line fitting these median values would add needless complexity and error.

There is little statistical difference between the inner and outer cut Gaussian fits to the spiral distributions reported in Table 2, the inner cut having a marginally tighter scatter. The tail in the outer cut’s distribution (see Fig. 4) also takes that distribution away from a true Gaussian. Given the tight scatter and more Gaussian distribution for the inner cut, we take the result  $\langle c/a \rangle = 0.124 \pm 0.001$  (stat)  $\pm 0.033$  (intrinsic/systematic) as most representative for the intrinsic flatness of spiral galaxies.

Our result agrees well with the non-parametric studies (see Sec. 2) of Guthrie (1992), based on micrometer measurements, and Giovanelli et al. (1994), who did not provide uncertainties.

### 6.2. *The Effectiveness of the Method of Characteristic Cuts*

To assess whether the method of characteristic cuts produces the most accurate measurements of intrinsic flattening, we compared our results to those derived from the more straightforward method of choosing a singular isophote. A traditional isophotal reference is  $\mu_B = 25$  mag arcsec<sup>-2</sup>. Fig. 12 shows the error-weighted distribution of our sample spiral and lenticular’s intrinsic flattening measured from the isophote of radius  $r = r_{25}$ , or whichever isophote whose radius was closest to  $r_{25}$ .

Comparing the properties of this distribution (see Fig. 12’s caption) with those derived from our method of characteristic cuts (see Table 2), our method, especially as applied to the inner cut, is found to minimize uncertainties and yield lower variance in  $c/a$  for both the spiral and lenticular galaxies. In short, a singular isophote traces heterogeneous structure resulting in a poorer tracer of intrinsic disk thickness. Furthermore, outer isophotes are more susceptible to lower S/N and perturbations. Our method based on characteristic cuts avoids these issues.

We have further compared the correlations between the structural parameters explored in Sec. 5.2 with those in Table 4. We tested for correlations between  $c/a|_{r_{25}}$  and these parameters. Cross-referencing the resulting correlations against Table 4 showed no significant changes. We conclude that our method of characteristic cuts yields a  $c/a$  distribution that is tighter than that of previous techniques, including Sec. 6.3 below.

### 6.3. *Parametric Decompositions as Measures of Intrinsic Flattening*

In principle, the ratio  $z_0/h$  can also be used to assess the global flattening of galaxy disks, provided the disk structures are well described by the adopted models. In Sec. 5.3, we already assessed that neither the thin nor thick disk  $z_0/h$

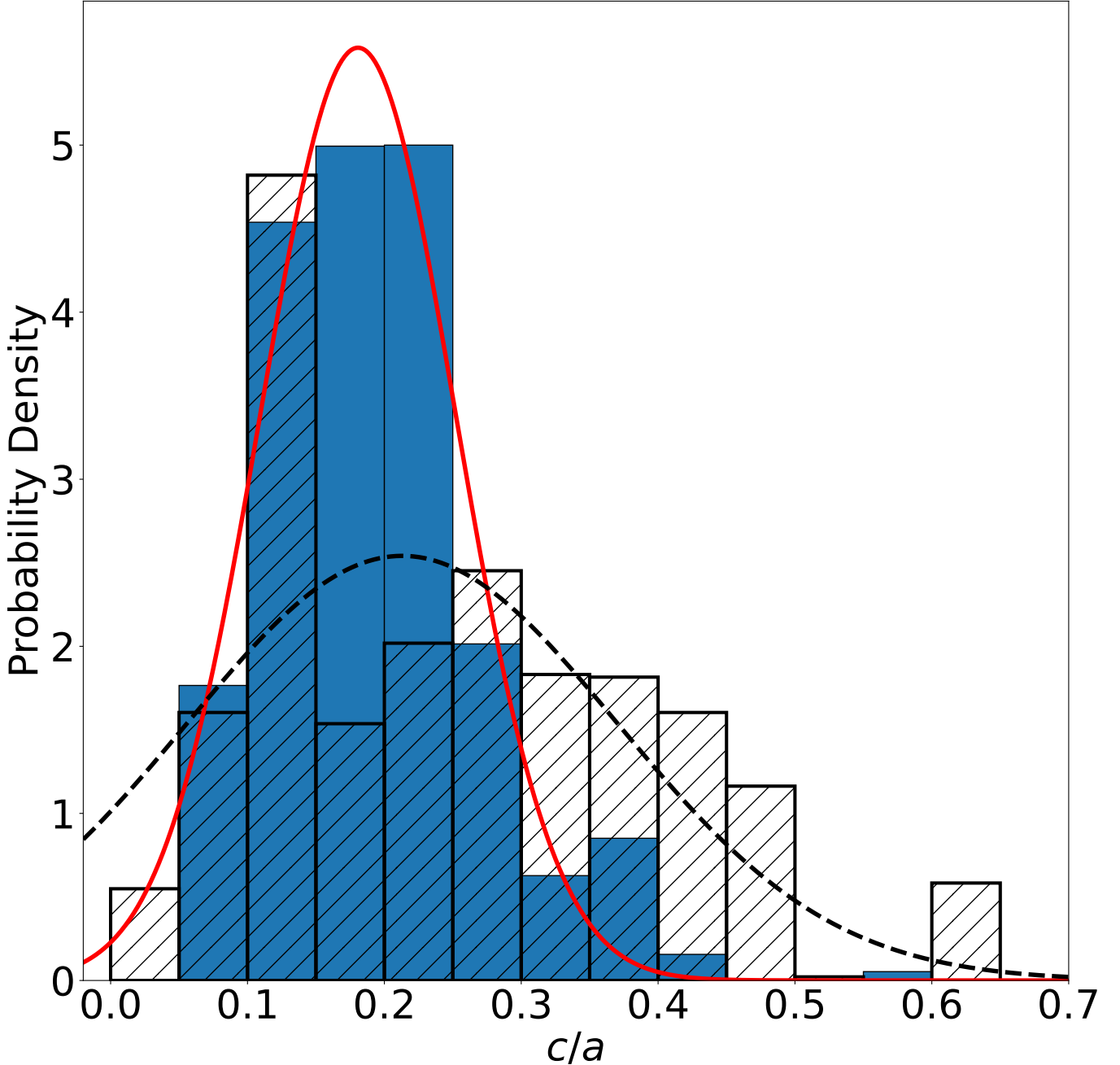


**Figure 12.** Distribution of intrinsic flattening measured at  $r = a = r_{25}$ , for the spiral and lenticular populations. The solid blue and hatched histograms represent the distribution of spiral and lenticular galaxies, respectively. The solid red and dashed lines are Gaussian fits to the spiral and lenticular distributions with  $\mu(Sp) = 0.175 \pm 0.003$  and  $\sigma = 0.071 \pm 0.002$  and  $\mu(S0) = 0.21 \pm 0.03$  and  $\sigma = 0.16 \pm 0.02$ , respectively.

map closely into  $c/a$ . However, the small range of  $z_0/h$  values for the thin disk offers a valuable comparison with our  $c/a$  values.

Fig. 13 shows the distributions of  $z_0/h$  values for the thin and thick disk scale heights. Our final estimate for the intrinsic  $c/a$  ought to lie somewhere between the values of  $z_0/h$  for the thin and thick disk, as is indeed found here. Gaussian fits to these distributions for spiral galaxies yield a mean flattening ratio for the thin disk of  $\langle z_{0,\text{thin}}/h \rangle \approx 0.08$  and thick disk  $\langle z_{0,\text{thick}}/h \rangle \approx 0.30$ . These are viewed as lower and upper limits for the intrinsic flattening of galaxy disks. In a multiple disk system, the intrinsic flattening might roughly correspond to the superposition of thin and

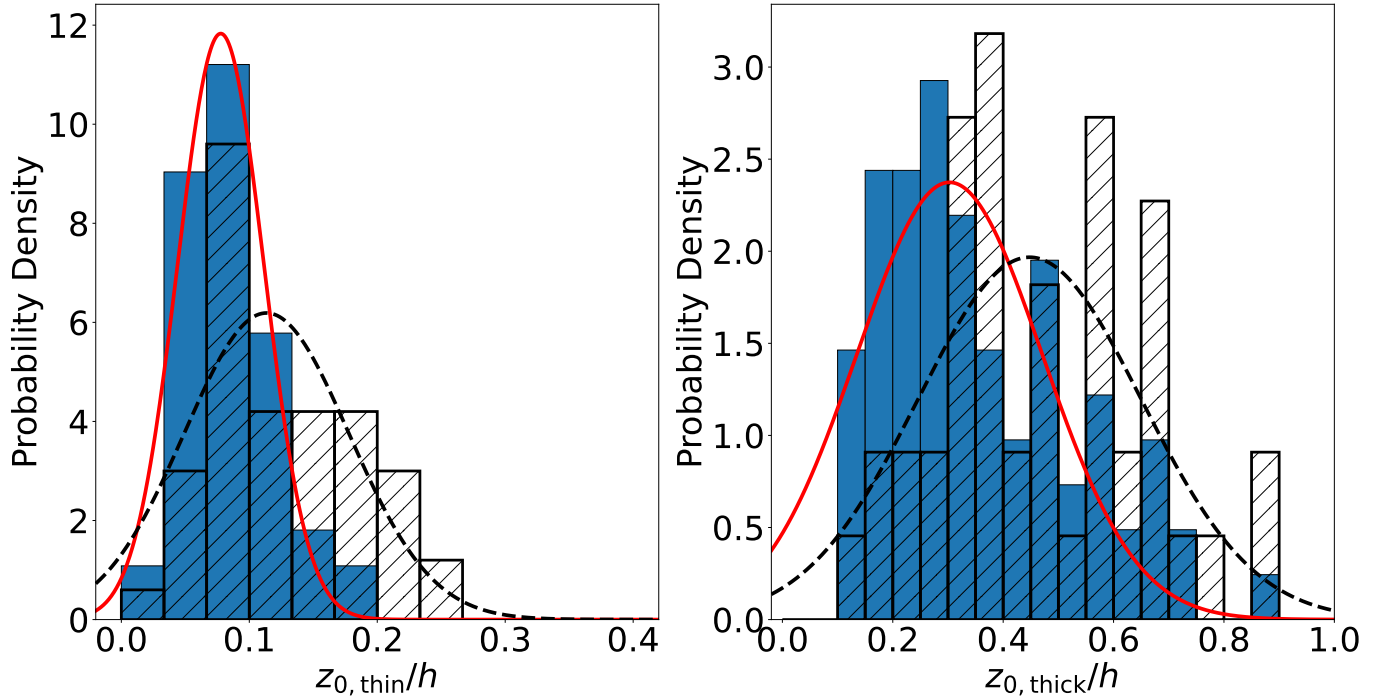


**Figure 13.** Histograms of the distributions of  $z_0/h$  for thin (left) and thick (right) disks. The solid blue histograms are the distributions of spiral galaxy  $z_0/h$ , and the hatched histograms are the distributions of lenticular galaxy  $z_0/h$ . Left: The solid red line is a Gaussian fit to the spiral distribution with  $\mu = 0.078 \pm 0.001$  and  $\sigma = 0.034 \pm 0.001$ . The dashed line is a Gaussian fit to the lenticular distribution with  $\mu = 0.113 \pm 0.008$  and  $\sigma = 0.064 \pm 0.007$ . Right: The solid red line is a Gaussian fit to the spiral distribution with  $\mu = 0.30 \pm 0.02$  and  $\sigma = 0.17 \pm 0.02$ . The dashed line is a Gaussian fit to the lenticular distribution with  $\mu = 0.45 \pm 0.04$  and  $\sigma = 0.20 \pm 0.03$ .

thick disk parameters, so in a galaxy with a thin/thick disk dichotomy,  $c/a$  should be greater than  $z_{0,\text{thin}}/h$ . The thin disk value is slightly smaller than our reported mean  $c/a$ , providing some assurance that our method of characteristic cuts truly measures intrinsic flattening. This exercise suggests that we have converged on a rather accurate estimate for the intrinsic flattening of spiral galaxies.

The Gaussian fits also show broader distributions of  $z_0/h$ , with a superposition of  $\sigma_{\text{thin}} = 0.03$  and  $\sigma_{\text{thick}} = 0.17$ , while  $c/a$  is measured with a single deviation of 0.03. Once again this supports using characteristic cuts to measure of the disk intrinsic thickness since it produces scatter comparable to the parametric  $z_0/h$  via a simpler method.

Furthermore, our  $\langle c/a \rangle$  value agrees well with the  $\langle z_0/h \rangle$  reported by each of Kregel et al. (2002), Hernandez & Cervantes-Sodi (2006), Mosenkov et al. (2015), and Mosenkov et al. (2022). That we arrive to the same intrinsic flattening with a simpler model-independent technique highlights the value and benefits of our method.

## 7. FUTURE WORK

As analytical methods evolve, so does the quality of datasets. The proposed method of characteristic cuts to constrain the intrinsic flattening of galaxy disks will certainly benefit from greater sample sizes. A ten-fold increase in the size of our sample, especially for the lenticulars, would go a long way towards characterizing the changes of disk thickening with Hubble type.

Considering the current data set, the S<sup>4</sup>G images were reduced over a series of five pipelines (Sheth et al. 2010; Muñoz-Mateos et al. 2015; Salo et al. 2015; Querejeta et al. 2015) to produce a variety of science-ready data products. In this study we analyzed maps from Pipeline 1 and used masks from Pipeline 2, but additional products, such as independent measurements of axial ratios and stellar emission maps, may prove valuable to further validate our findings. For instance, the S<sup>4</sup>G Pipeline 5 (Querejeta et al. 2015) separated galaxy images into stellar and dust emission maps using the Independent Component Analysis method of Meidt et al. (2012). The effects of dust on the characteristic cuts used in this study could be assessed by repeating our analysis using these stellar emission maps,

thereby quantifying the flattening of isophotes caused by dust emission. However, the use of such maps might introduce model-dependences that we aimed to avoid.

The foundation for the estimation of disk intrinsic flattening from face-on view (e.g., Giovanelli et al. 1994) is an ad-hoc formulation that assumes the observed flux varies linearly with  $a_{\text{obs}}/c_{\text{obs}}$ . Empirical measurements of inclination effects cannot be made via direct observations. Instead, galaxy simulations could be observed to characterize individual systems from multiple angles. For instance, the Numerical Investigation of a Hundred Astrophysical Objects project (NIHAO; Wang et al. 2015) provides impressive access to a wide variety of simulated galaxy types. Mock observations of NIHAO disk galaxies at various inclination angles, primarily focused around near face- and edge-on perspectives, offer an ideal data set with which to (i) repeat this analysis and verify our results, and (ii) derive an empirical formulation of the inclination effects on isophotal radii and observed axis ratios (e.g., Byun et al. 1994; Agertz et al. 2013; Roškar et al. 2014).

## 8. SUMMARY

Defining the size of a galaxy based on its projected image on the sky is especially challenging and requires care. We have proposed the method of characteristic cuts for measuring the intrinsic flattening of disk galaxies and applied it to a sample of 141 (nearly) edge-on galaxies from the S<sup>4</sup>G imaged in 3.6  $\mu\text{m}$ . We used AutoProf, a Python-based automated tool for the photometry of astronomical images (Stone et al. 2021), to perform isophotal fits on the 3.6  $\mu\text{m}$  images of each galaxy. With these isophotes, we established the characteristic cuts of each galaxy by taking the average axial ratio  $c/a$  of isophotes falling within axial cuts of  $0.2 r_{25} \leq |a| \leq 0.5 r_{25}$  and  $0.5 r_{25} \leq |a| \leq 0.8 r_{25}$ , which we referred to as the inner and outer cuts, respectively. Those galaxies which showed clear visual indications of poor fits or had large  $c/a$  variances within either cut were rejected, leaving us with a sample of 133 galaxies with good fits. We also retrieved surface brightness profiles and thin and thick disks decompositions from Comerón et al. (2018) in addition to various physical parameters from Muñoz-Mateos et al. (2015). Our findings are summarized here:

1. Spiral galaxies follow a universal intrinsic disk flattening with a mean value of  $\langle c/a \rangle = 0.124 \pm 0.002$  and standard deviation  $\sigma = 0.034 \pm 0.001$ .
2. For lenticular galaxies, the  $c/a$  distribution is broader, with standard deviation  $\sigma = 0.13 \pm 0.02$  and, after averaging the inner and outer cuts, is centered on  $\langle c/a \rangle = 0.20 \pm 0.04$ . For  $T < 3$ ,  $c/a$  negatively correlates with  $T$ , whereas  $c/a$  is independent of  $T$  for  $T > 3$ . Lenticular galaxies show a conspicuously strong negative correlation with Hubble type, though the scatter in  $c/a$  is too large to make definitive claims about the evolution of their disks. Galaxies with bars do not appear significantly thicker than those without, though barred systems in our sample are too few to claim that this is a true meaningful difference.
3. While largely insensitive to any galaxy structural parameter, including circular velocity, the intrinsic flattening of galaxy disks shows a tentative correlation with  $\log C_{31}$ , in the sense that bulge and disk growth are linked (Courteau 1996; Kormendy & Kennicutt 2004; Comerón et al. 2014).
4. The scale height,  $z$ , correlates well with the vertical size  $c$ , and the scale length,  $h$ , correlates well with the semi-major axis length,  $a$ , but the ration of  $z/h$  does not correlate well with  $c/a$ .

## 9. ACKNOWLEDGMENTS

This research project was initiated under the watchful eye of Simon Díaz García. We are grateful for his precious suggestions and contributions. Peter Erwin is also thanked for insightful discussions and references. SC(Canada) and CS acknowledge generous support from the Natural Sciences and Engineering Research Council of Canada and Queen’s University through various scholarships and grants. CS also acknowledges support from the Canadian Institute for Theoretical Astrophysics (CITA) National Fellowship program. SC(Spain) also acknowledges funding from the State Research Agency (AEI-MCINN) of the Spanish Ministry of Science and Innovation under the grant “Thick discs, relics of the infancy of galaxies” with reference PID2020-113213GA-I00.

## APPENDIX

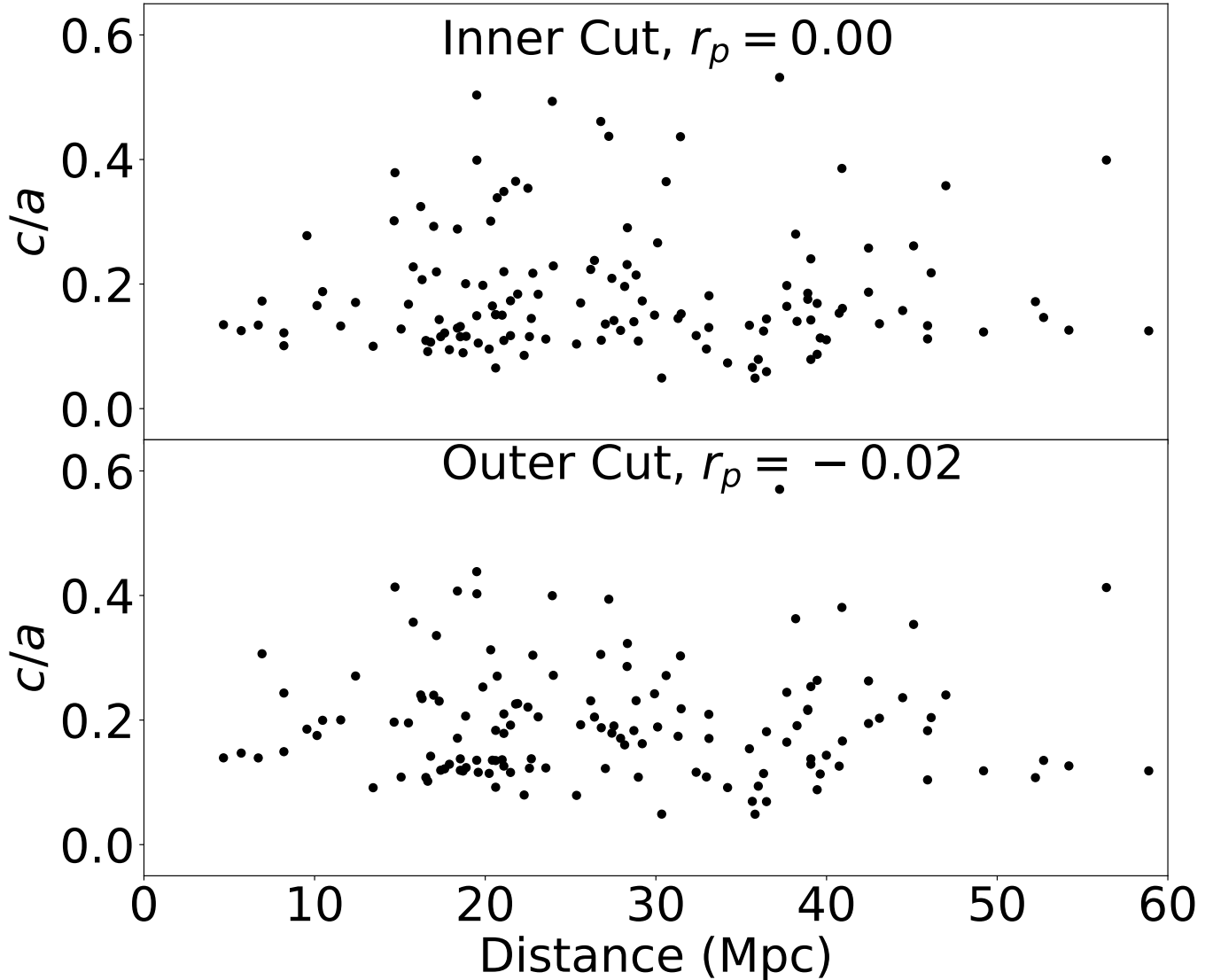


**Figure 14.** Intrinsic flattening of the inner (top) and outer (bottom) cuts as a function of distance.

#### A. RESOLUTION EFFECTS AND PSF

$S^4G$  galaxies are  $\sim 5$  to 60 Mpc away from us. To identify whether our analysis suffers any proximity bias, Fig. 14 plots intrinsic flattening  $c/a$  of  $S^4G$  edge-on galaxies as a function of distance. Qualitative and quantitative inspections of Fig. 14 show that our intrinsic flattening values are independent of distance and thus free of resolution effects. Therefore, distances do not bias our results through resolution effects.

Our study did not account for PSF effects which could introduce scattered light from the bulge or midplane into the disk’s extended structure. Such a treatment could employ the IRAC PSF of Hora et al. (2012). A symmetrised version of this PSF is required for such an effort, as all  $S^4G$  images are composed of two visits to each galaxy at different orientations by the *Spitzer* Space Telescope. An azimuthally averaged PSF would be needed to deconvolve our images.

While the exploration of PSF effects is beyond the scope of the current paper, we can alleviate most concerns by comparing the scale of an approximate PSF to the shortest scale studied here. We used a  $2.1''$  FWHM Gaussian as an approximation for the  $S^4G$  PSF. The shortest scale studied is the semi-minor axis of the inner cut. These scales are compared by taking the ratio of  $c$  to half the PSF FWHM, or  $2c_{\text{inner}}/2.1''$ , as shown in the log-binned histogram of Fig. 15. For this ratio to be close to or less than one, the light scattered by the PSF would be of some concern. Fig. 15 suggests that our results do not suffer significantly from PSF induced scattered light. The mean value of the



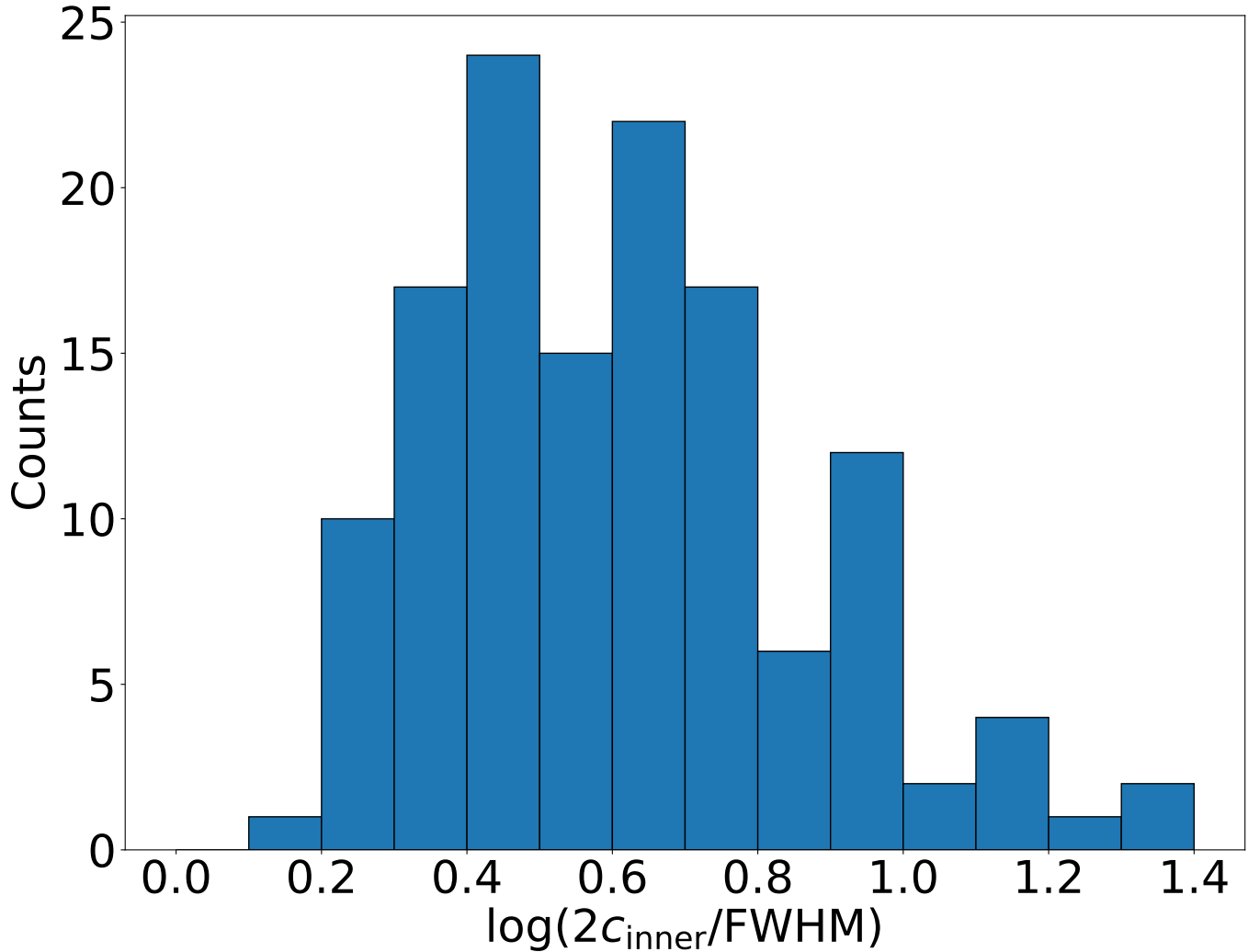


**Figure 15.** Histogram of the ratio  $c$  from the inner cuts over the PSF FWHM.

ratio  $2c_{\text{inner}}/2.1''$  is 4.9, with a smallest value of 1.6. Still, a future analysis the distribution of  $c/a$  ought to explore this question more closely.

#### REFERENCES

- Adelman-McCarthy, J. K., Agüeros, M. A., Allam, S. S., et al. 2008, *ApJS*, 175, 297, doi: [10.1086/524984](https://doi.org/10.1086/524984)
- Agertz, O., Kravtsov, A. V., Leitner, S. N., & Gnedin, N. Y. 2013, *ApJ*, 770, 25, doi: [10.1088/0004-637X/770/1/25](https://doi.org/10.1088/0004-637X/770/1/25)
- Alam, S. M. K., & Ryden, B. S. 2002, *ApJ*, 570, 610, doi: [10.1086/339790](https://doi.org/10.1086/339790)
- Arora, N., Stone, C., Courteau, S., & Jarrett, T. H. 2021, *MNRAS*, 505, 3135, doi: [10.1093/mnras/stab1430](https://doi.org/10.1093/mnras/stab1430)
- Binney, J., & de Vaucouleurs, G. 1981, *MNRAS*, 194, 679, doi: [10.1093/mnras/194.3.679](https://doi.org/10.1093/mnras/194.3.679)
- Bizyaev, D. V., Kautsch, S. J., Mosenkov, A. V., et al. 2014, *ApJ*, 787, 24, doi: [10.1088/0004-637X/787/1/24](https://doi.org/10.1088/0004-637X/787/1/24)
- Buck, T., Obreja, A., Macciò, A. V., et al. 2020, *MNRAS*, 491, 3461, doi: [10.1093/mnras/stz3241](https://doi.org/10.1093/mnras/stz3241)
- Buta, R. J., Sheth, K., Athanassoula, E., et al. 2015, *ApJS*, 217, 32, doi: [10.1088/0067-0049/217/2/32](https://doi.org/10.1088/0067-0049/217/2/32)
- Byun, Y. I., Freeman, K. C., & Kylafis, N. D. 1994, *ApJ*, 432, 114, doi: [10.1086/174553](https://doi.org/10.1086/174553)
- Cluver, M. E., Jarrett, T. H., Hopkins, A. M., et al. 2014, *ApJ*, 782, 90, doi: [10.1088/0004-637X/782/2/90](https://doi.org/10.1088/0004-637X/782/2/90)
- Comerón, S., Elmegreen, B. G., Salo, H., et al. 2014, *A&A*, 571, A58, doi: [10.1051/0004-6361/201424412](https://doi.org/10.1051/0004-6361/201424412)
- Comerón, S., Salo, H., & Knapen, J. H. 2018, *A&A*, 610, A5, doi: [10.1051/0004-6361/201731415](https://doi.org/10.1051/0004-6361/201731415)

- Comerón, S., Salo, H., Peletier, R. F., & Mentz, J. 2016, *A&A*, 593, L6, doi: [10.1051/0004-6361/201629292](https://doi.org/10.1051/0004-6361/201629292)
- Comerón, S., Knapen, J. H., Sheth, K., et al. 2011a, *ApJ*, 729, 18, doi: [10.1088/0004-637X/729/1/18](https://doi.org/10.1088/0004-637X/729/1/18)
- Comerón, S., Elmegreen, B. G., Knapen, J. H., et al. 2011b, *ApJL*, 738, L17, doi: [10.1088/2041-8205/738/2/L17](https://doi.org/10.1088/2041-8205/738/2/L17)
- . 2011c, *ApJ*, 741, 28, doi: [10.1088/0004-637X/741/1/28](https://doi.org/10.1088/0004-637X/741/1/28)
- Comerón, S., Elmegreen, B. G., Salo, H., et al. 2012, *ApJ*, 759, 98, doi: [10.1088/0004-637X/759/2/98](https://doi.org/10.1088/0004-637X/759/2/98)
- Conroy, C. 2013, *ARA&A*, 51, 393, doi: [10.1146/annurev-astro-082812-141017](https://doi.org/10.1146/annurev-astro-082812-141017)
- Courteau, S. 1996, *ApJS*, 103, 363, doi: [10.1086/192281](https://doi.org/10.1086/192281)
- Courteau, S., Cappellari, M., de Jong, R. S., et al. 2014, *Reviews of Modern Physics*, 86, 47, doi: [10.1103/RevModPhys.86.47](https://doi.org/10.1103/RevModPhys.86.47)
- Dahari, O. 1984, *AJ*, 89, 966, doi: [10.1086/113591](https://doi.org/10.1086/113591)
- Dalcanton, J. J., Yoachim, P., & Bernstein, R. A. 2004, *ApJ*, 608, 189, doi: [10.1086/386358](https://doi.org/10.1086/386358)
- de Grijs, R. 1998, *MNRAS*, 299, 595, doi: [10.1046/j.1365-8711.1998.01896.x](https://doi.org/10.1046/j.1365-8711.1998.01896.x)
- de Grijs, R., Peletier, R. F., & van der Kruit, P. C. 1997, *A&A*, 327, 966, doi: [10.48550/arXiv.astro-ph/9707074](https://doi.org/10.48550/arXiv.astro-ph/9707074)
- de Vaucouleurs, G. H., de Vaucouleurs, A., & Shapley, H. 1964, *Reference catalogue of bright galaxies* (Austin, TX: University of Texas Press)
- Díaz-García, S., Comerón, S., Courteau, S., et al. 2022, *A&A*, 667, A109, doi: [10.1051/0004-6361/202142447](https://doi.org/10.1051/0004-6361/202142447)
- Doore, K., Eufrazio, R. T., Lehmer, B. D., et al. 2021, *ApJ*, 923, 26, doi: [10.3847/1538-4357/ac25f3](https://doi.org/10.3847/1538-4357/ac25f3)
- Erwin, P. 2015, *ApJ*, 799, 226, doi: [10.1088/0004-637X/799/2/226](https://doi.org/10.1088/0004-637X/799/2/226)
- Erwin, P., Beckman, J. E., & Pohlen, M. 2005, *ApJL*, 626, L81, doi: [10.1086/431739](https://doi.org/10.1086/431739)
- Erwin, P., Pohlen, M., & Beckman, J. E. 2008, *AJ*, 135, 20, doi: [10.1088/0004-6256/135/1/20](https://doi.org/10.1088/0004-6256/135/1/20)
- Eskew, M., Zaritsky, D., & Meidt, S. 2012, *AJ*, 143, 139, doi: [10.1088/0004-6256/143/6/139](https://doi.org/10.1088/0004-6256/143/6/139)
- Fasano, G., Amico, P., Bertola, F., Vio, R., & Zeilinger, W. W. 1993, *MNRAS*, 262, 109, doi: [10.1093/mnras/262.1.109](https://doi.org/10.1093/mnras/262.1.109)
- Fazio, G. G., Hora, J. L., Allen, L. E., et al. 2004, *ApJS*, 154, 10, doi: [10.1086/422843](https://doi.org/10.1086/422843)
- Freeman, K. C. 1970, *ApJ*, 160, 811, doi: [10.1086/150474](https://doi.org/10.1086/150474)
- García de la Cruz, J., Martig, M., & Minchev, I. 2023, *MNRAS*, 518, 5403, doi: [10.1093/mnras/stac3371](https://doi.org/10.1093/mnras/stac3371)
- Gilmore, G., & Reid, N. 1983, *MNRAS*, 202, 1025, doi: [10.1093/mnras/202.4.1025](https://doi.org/10.1093/mnras/202.4.1025)
- Giovanelli, R., & Haynes, M. P. 1988, in *Galactic and Extragalactic Radio Astronomy*, ed. K. I. Kellermann & G. L. Verschuur (Berlin:Springer), 522–562
- Giovanelli, R., Haynes, M. P., Salzer, J. J., et al. 1994, *AJ*, 107, 2036, doi: [10.1086/117014](https://doi.org/10.1086/117014)
- Guthrie, B. N. G. 1992, *A&AS*, 93, 255
- Hall, C., Courteau, S., Jarrett, T., et al. 2018, *ApJ*, 865, 154, doi: [10.3847/1538-4357/aadee1](https://doi.org/10.3847/1538-4357/aadee1)
- Haynes, M. P., & Giovanelli, R. 1984, *AJ*, 89, 758, doi: [10.1086/113573](https://doi.org/10.1086/113573)
- Hernandez, X., & Cervantes-Sodi, B. 2006, *MNRAS*, 368, 351, doi: [10.1111/j.1365-2966.2006.10115.x](https://doi.org/10.1111/j.1365-2966.2006.10115.x)
- Holmberg, E. 1946, *Meddelanden fran Lunds Astronomiska Observatorium Serie II*, 117, 3
- Hopkins, P. F., Gurvich, A. B., Shen, X., et al. 2023, *MNRAS*, 525, 2241, doi: [10.1093/mnras/stad1902](https://doi.org/10.1093/mnras/stad1902)
- Hora, J. L., Marengo, M., Park, R., et al. 2012, 8442, doi: [10.1117/12.926894](https://doi.org/10.1117/12.926894)
- Hubble, E. P. 1926, *ApJ*, 64, 321, doi: [10.1086/143018](https://doi.org/10.1086/143018)
- Kautsch, S. J., Gallagher, J. S., & Grebel, E. K. 2009, *Astronomische Nachrichten*, 330, 1056, doi: [10.1002/asna.200911292](https://doi.org/10.1002/asna.200911292)
- Knapen, J. H., & van der Kruit, P. C. 1991, *A&A*, 248, 57
- Kormendy, J., & Kennicutt, Robert C., J. 2004, *ARA&A*, 42, 603, doi: [10.1146/annurev.astro.42.053102.134024](https://doi.org/10.1146/annurev.astro.42.053102.134024)
- Kregel, M., van der Kruit, P. C., & de Grijs, R. 2002, *MNRAS*, 334, 646, doi: [10.1046/j.1365-8711.2002.05556.x](https://doi.org/10.1046/j.1365-8711.2002.05556.x)
- Kregel, M., van der Kruit, P. C., & Freeman, K. C. 2004, *MNRAS*, 351, 1247, doi: [10.1111/j.1365-2966.2004.07864.x](https://doi.org/10.1111/j.1365-2966.2004.07864.x)
- Laine, J., Laurikainen, E., Salo, H., et al. 2014, *MNRAS*, 441, 1992, doi: [10.1093/mnras/stu628](https://doi.org/10.1093/mnras/stu628)
- Lambas, D. G., Maddox, S. J., & Loveday, J. 1992, *MNRAS*, 258, 404, doi: [10.1093/mnras/258.2.404](https://doi.org/10.1093/mnras/258.2.404)
- Lintott, C. J., Schawinski, K., Slosar, A., et al. 2008, *MNRAS*, 389, 1179, doi: [10.1111/j.1365-2966.2008.13689.x](https://doi.org/10.1111/j.1365-2966.2008.13689.x)
- Loveday, J. N. J. 1989, PhD thesis, University of Cambridge, UK
- MacArthur, L. A., Courteau, S., & Holtzman, J. A. 2003, *ApJ*, 582, 689, doi: [10.1086/344506](https://doi.org/10.1086/344506)
- Makarov, D., Prugniel, P., Terekhova, N., Courtois, H., & Vaughn, I. 2014, *A&A*, 570, A13, doi: [10.1051/0004-6361/201423496](https://doi.org/10.1051/0004-6361/201423496)
- Meidt, S. E., Schinnerer, E., Knapen, J. H., et al. 2012, *ApJ*, 744, 17, doi: [10.1088/0004-637X/744/1/17](https://doi.org/10.1088/0004-637X/744/1/17)
- Meidt, S. E., Schinnerer, E., van de Ven, G., et al. 2014, *ApJ*, 788, 144, doi: [10.1088/0004-637X/788/2/144](https://doi.org/10.1088/0004-637X/788/2/144)
- Meng, X., & Gnedin, O. Y. 2021, *MNRAS*, 502, 1433, doi: [10.1093/mnras/stab088](https://doi.org/10.1093/mnras/stab088)
- Mosenkov, A. V., Sotnikova, N. Y., Reshetnikov, V. P., Bizyaev, D. V., & Kautsch, S. J. 2015, *MNRAS*, 451, 2376, doi: [10.1093/mnras/stv1085](https://doi.org/10.1093/mnras/stv1085)

- Mosenkov, A. V., Usachev, P. A., Shakespear, Z., et al. 2022, *MNRAS*, 515, 5698, doi: [10.1093/mnras/stac2112](https://doi.org/10.1093/mnras/stac2112)
- Muñoz-Mateos, J. C., Sheth, K., Regan, M., et al. 2015, *ApJS*, 219, 3, doi: [10.1088/0067-0049/219/1/3](https://doi.org/10.1088/0067-0049/219/1/3)
- Nilson, P. 1973, *Uppsala general catalogue of galaxies* (Uppsala: Astronomiska Observatorium)
- Olling, R. P. 1995, *AJ*, 110, 591, doi: [10.1086/117545](https://doi.org/10.1086/117545)
- Ossa-Fuentes, L., Borlaff, A. S., Beckman, J. E., Marcum, P. M., & Fanelli, M. N. 2023, *ApJ*, 951, 149, doi: [10.3847/1538-4357/acd54c](https://doi.org/10.3847/1538-4357/acd54c)
- Padilla, N. D., & Strauss, M. A. 2008, *MNRAS*, 388, 1321, doi: [10.1111/j.1365-2966.2008.13480.x](https://doi.org/10.1111/j.1365-2966.2008.13480.x)
- Pinna, F., Falcón-Barroso, J., Martig, M., et al. 2019a, *A&A*, 623, A19, doi: [10.1051/0004-6361/201833193](https://doi.org/10.1051/0004-6361/201833193)
- . 2019b, *A&A*, 625, A95, doi: [10.1051/0004-6361/201935154](https://doi.org/10.1051/0004-6361/201935154)
- Pohlen, M., Beckman, J. E., Hüttemeister, S., et al. 2004, in *Astrophysics and Space Science Library*, Vol. 319, *Penetrating Bars Through Masks of Cosmic Dust*, ed. D. L. Block, I. Puerari, K. C. Freeman, R. Groess, & E. K. Block, 713, doi: [10.1007/978-1-4020-2862-5\\_61](https://doi.org/10.1007/978-1-4020-2862-5_61)
- Pohlen, M., & Trujillo, I. 2006, *A&A*, 454, 759, doi: [10.1051/0004-6361:20064883](https://doi.org/10.1051/0004-6361:20064883)
- Querejeta, M., Meidt, S. E., Schinnerer, E., et al. 2015, *ApJS*, 219, 5, doi: [10.1088/0067-0049/219/1/5](https://doi.org/10.1088/0067-0049/219/1/5)
- Rix, H.-W., & Rieke, M. J. 1993, *ApJ*, 418, 123, doi: [10.1086/173376](https://doi.org/10.1086/173376)
- Roškar, R., Teyssier, R., Agertz, O., Wetzstein, M., & Moore, B. 2014, *MNRAS*, 444, 2837, doi: [10.1093/mnras/stu1548](https://doi.org/10.1093/mnras/stu1548)
- Ryden, B. S. 2004, *ApJ*, 601, 214, doi: [10.1086/380437](https://doi.org/10.1086/380437)
- S4G Team. 2020, *Spitzer Survey of Stellar Structure in Galaxies Catalog*, IPAC, doi: [10.26131/IRSA335](https://doi.org/10.26131/IRSA335)
- Salo, H., Laurikainen, E., Laine, J., et al. 2015, *ApJS*, 219, 4, doi: [10.1088/0067-0049/219/1/4](https://doi.org/10.1088/0067-0049/219/1/4)
- Sandage, A., Freeman, K. C., & Stokes, N. R. 1970, *ApJ*, 160, 831, doi: [10.1086/150475](https://doi.org/10.1086/150475)
- Sandin, C. 2014, *A&A*, 567, A97, doi: [10.1051/0004-6361/201423429](https://doi.org/10.1051/0004-6361/201423429)
- . 2015, *A&A*, 577, A106, doi: [10.1051/0004-6361/201425168](https://doi.org/10.1051/0004-6361/201425168)
- Sheth, K., Regan, M., Hinz, J. L., et al. 2010, *PASP*, 122, 1397, doi: [10.1086/657638](https://doi.org/10.1086/657638)
- Shibuya, T., Ouchi, M., & Harikane, Y. 2015, *ApJS*, 219, 15, doi: [10.1088/0067-0049/219/2/15](https://doi.org/10.1088/0067-0049/219/2/15)
- Sotillo-Ramos, D., Pillepich, A., Donnari, M., et al. 2022, *MNRAS*, 516, 5404, doi: [10.1093/mnras/stac2586](https://doi.org/10.1093/mnras/stac2586)
- Stark, D. V., McGaugh, S. S., & Swaters, R. A. 2009, *AJ*, 138, 392, doi: [10.1088/0004-6256/138/2/392](https://doi.org/10.1088/0004-6256/138/2/392)
- Stone, C. J., Arora, N., Courteau, S., & Cuillandre, J.-C. 2021, *MNRAS*, 508, 1870, doi: [10.1093/mnras/stab2709](https://doi.org/10.1093/mnras/stab2709)
- Tikhonov, N. A., & Galazutdinova, O. A. 2005, *Astrophysics*, 48, 221, doi: [10.1007/s10511-005-0021-8](https://doi.org/10.1007/s10511-005-0021-8)
- Toth, G., & Ostriker, J. P. 1992, *ApJ*, 389, 5, doi: [10.1086/171185](https://doi.org/10.1086/171185)
- Trujillo, I., Chamba, N., & Knapen, J. H. 2020, *MNRAS*, 493, 87, doi: [10.1093/mnras/staa236](https://doi.org/10.1093/mnras/staa236)
- Tully, R. B., Rizzi, L., Shaya, E. J., et al. 2009, *AJ*, 138, 323, doi: [10.1088/0004-6256/138/2/323](https://doi.org/10.1088/0004-6256/138/2/323)
- Untertorn, C. T., & Ryden, B. S. 2008, *ApJ*, 687, 976, doi: [10.1086/591898](https://doi.org/10.1086/591898)
- van der Kruit, P. C., & Freeman, K. C. 2011, *ARA&A*, 49, 301, doi: [10.1146/annurev-astro-083109-153241](https://doi.org/10.1146/annurev-astro-083109-153241)
- van der Kruit, P. C., & Searle, L. 1981, *A&A*, 95, 105
- van der Wel, A., Bell, E. F., Häussler, B., et al. 2012, *ApJS*, 203, 24, doi: [10.1088/0067-0049/203/2/24](https://doi.org/10.1088/0067-0049/203/2/24)
- Vázquez-Mata, J. A., Hernández-Toledo, H. M., Avila-Reese, V., et al. 2022, *MNRAS*, 512, 2222, doi: [10.1093/mnras/stac635](https://doi.org/10.1093/mnras/stac635)
- Vera, M., Alonso, S., & Coldwell, G. 2016, *A&A*, 595, A63, doi: [10.1051/0004-6361/201628750](https://doi.org/10.1051/0004-6361/201628750)
- Wang, L., Dutton, A. A., Stinson, G. S., et al. 2015, *MNRAS*, 454, 83, doi: [10.1093/mnras/stv1937](https://doi.org/10.1093/mnras/stv1937)
- Watkins, A. E., Salo, H., Laurikainen, E., et al. 2022, *A&A*, 660, A69, doi: [10.1051/0004-6361/202142627](https://doi.org/10.1051/0004-6361/202142627)
- Werner, M. W., Roellig, T. L., Low, F. J., et al. 2004, *ApJS*, 154, 1, doi: [10.1086/422992](https://doi.org/10.1086/422992)
- Yoachim, P., & Dalcanton, J. J. 2006, *AJ*, 131, 226, doi: [10.1086/497970](https://doi.org/10.1086/497970)
- York, D. G., Adelman, J., Anderson, John E., J., et al. 2000, *AJ*, 120, 1579, doi: [10.1086/301513](https://doi.org/10.1086/301513)